A High Resolution Staw Tube Tracker Near Detector for the LBNE Program

Principal Investigators: S. R. Mishra, R. Petti and C. Rosenfeld
Department of Physics and Astronomy
University of South Carolina
Columbia, SC 29208

1 Overview and Purpose

We propose a high-resolution neutrino experiment within a dipole magnetic field, HiResMnu [1] as the near detector (ND) for the long-baseline neutrino oscillation experiment(s) (LBNE) at the Deep Underground Science and Engineering Lab (DUSEL) at Homestake. Taking advantage of the unprecedented (anti)neutrino fluxes available at Fermilab for LBNE, HiResMnu combines the large statistics with high resolution in the reconstruction of neutrino events. The high resolution is an imperative to achieve the highest precision in the measurements of the elements of the neutrino mass matrix, and to have redundant measurements to establish a discovery should something entirely unexpected be observed in the FD. The proposed $4 \times 4 \times 7$ m^3 detector, inside a dipole magnetic field of $\boldsymbol{B \approx 0.4}$ T, will have the density of liquid hydrogen, $\boldsymbol{\rho \approx 0.1}$ gm/cm$^{\mathbf{3}}$, with a nominal fiducial mass of 7.4 tons. The proposed detector has two goals:

Constraining the systematic uncertainties in the LBNE oscillation measurements and searches: First we want to quantify the precision of ND measurements that will be essential for the neutrino oscillation studies ($\boldsymbol{\nu}$OSCL) in LBNE. Regardless of the process under study the systematic error should be less than the corresponding statistical error. Once we understand the precision needed in the ND, the focus will turn to the detector parameters that will ensure this precision. To this end we will pay particular attention to:—

(a): Measurement of the relative abundance and the energy spectrum of the **four** species of neutrinos in the LBNE-beam: $\boldsymbol{\nu_\mu}$, $\boldsymbol{\overline{\nu}_\mu}$, $\boldsymbol{\nu_e}$ and $\boldsymbol{\overline{\nu}_e}$ via the ***in situ*** identification of their CC-interactions;

(b): Determination of the absolute $\boldsymbol{\nu}$-flux using the $\boldsymbol{\nu}$-electron scattering;

(c) Identification and precise measurement of $\boldsymbol{\pi^0}$, photon, electron, and positron in $\boldsymbol{\nu}$-induced neutral-current (NC) and charge-current (CC) interactions, the most important background to the $\boldsymbol{\nu_e}$-appearance;

(d) Measurement of NC cross-section relative to CC as a function of $\boldsymbol{E_{Had}}$, since NC-processes constitute the largest background to the $\boldsymbol{\nu}$-CC identification;

(e) Measurement of $\boldsymbol{\pi^\pm}$ content in CC and NC hadronic jet since the $\boldsymbol{\pi^\pm \rightarrow \mu^\pm}$ is the principal background to the $\boldsymbol{\nu_\mu(\bar{\nu}_\mu)}$-CC;

(f) Mesurement of differential cross-section for various exclusive, semi-exclusive, and inclusive channels relevant for the $\boldsymbol{\nu}$OSCL studies; and

(g) Quantification of nuclear-target material cross-section which might effect the ν-nucleus interactions when extrapolating the ND measurements to the FD.

Precision standard model neutrino physics: We will determine the consistency of detector parameters, optimized for the LBNE oscillation studies, with a generational advance in the precision of standard model measurements. As a case study, we propose to investigate the feasibility of a measurement of the weak-mixing angle, $\sin^2\theta_W$ in the $\nu(\overline{\nu})$-q (DIS) channel at a momentum transfer (Q) in the neighborhood of 4 GeV with a precision approaching 0.2%. The sought precision on $\sin^2\theta_W$ in this experiment will be comparable to that attained by the collider experiments.

The proposed detector reinvents the concept of a near detector providing powerful constraints on the systematics associated with the discovery of the neutrino mixing matrix elements by the LBNE. It promises an "Event-Generator" measurement for the LBNE FD including the hadronic multiplicity ($\pi^{\pm}$, $K^{\pm}$, π^0 & p) comprising topologies of CC and Neutral-Current (NC) events with a special focus on the identification of of (semi)exclusive e^-, e^+, γ, relevant to the ν_e appearance. It concurrently offers a rich precision ν-physics program: questions/measurements that were speculative will be possible to address with the HiResMnu-idea. If realized the detector will yield over 75 papers and "textbook" measurements.

The report is organized as follows: Section 2 presents the detector concept; Section 3 presents the expected detector performance and sensitivity studies for a select sample of ν-interactions; Section 4 presents the detector dimensions, the power & cooling requirements, and the safety issues; Section 5 presents the planned and anticipated R&D studies; and Section **??** presents the CDR-forms which we have filled based upon our estimates.

2 The HiResMnu Detector

The proposed detector will have dimensions of $\mathbf{450 \times 450 \times 800}$ cm^3 embedded in a dipole magnet with $\mathbf{B \approx 0.4}$ T. The nominal fiducial volume (FV), $\mathbf{350 \times 350 \times 600}$ cm^3, corresponds to 7.4 tons of mass. A schematic of the HiResMν concept is presented in Figure 1; Figure 2 shows the layout with the external muon detector.

The HiResMnu idea builds upon the NOMAD-experience [2, 3, 4, 5]. NOMAD is a low-density tracking detector, $\rho \leq \mathbf{0.1}$ gm/cm^3, inside a B-field with a good electromagnetic carolimeter (ECAL) at the downstream end and, outside the magnet, a muon-detector. We propose an active target tracker with a factor of two more sampling points along the z-axis (ν-direction) and a factor of six more sampling points in the plane transverse to the neutrino compared to the NOMAD. Figure 3 juxtaposes the resolving power of the NOMAD detector with the massive CCFR/NuTeV calorimeter. One sees the contrast in resolution for an NC event candidate in the NuTeV experiment compared with one in NOMAD. The HiResMnu will increase, by an order of magnitude, the data points in tracking charged particles and the coverage for side-exiting neutrals. Taking advantage of the existing design and production details for the ATLAS Transition Radiation Tracker [6, 7, 8] and the COMPASS detector [9, 10], we are proposing straw-tube trackers (STT) for the HiResMnu. Figurefig-det-schematic shows one module of the STT. In what follows, we take the STT a default option for the active neutrino target. We would consider other technologies, but we are committed to a low-density, $\rho \leq \mathbf{0.1}$ gm/cm^3, precision tracker within a magnetic field. We have quantified the improvements over the NOMAD detector. These include:

(1) Tracking Detector: The tracker will be composed of straw tubes with 1 cm diameter. Vertical (Y) and horizontal (X) straws will be alternated and arranged in modules - each module

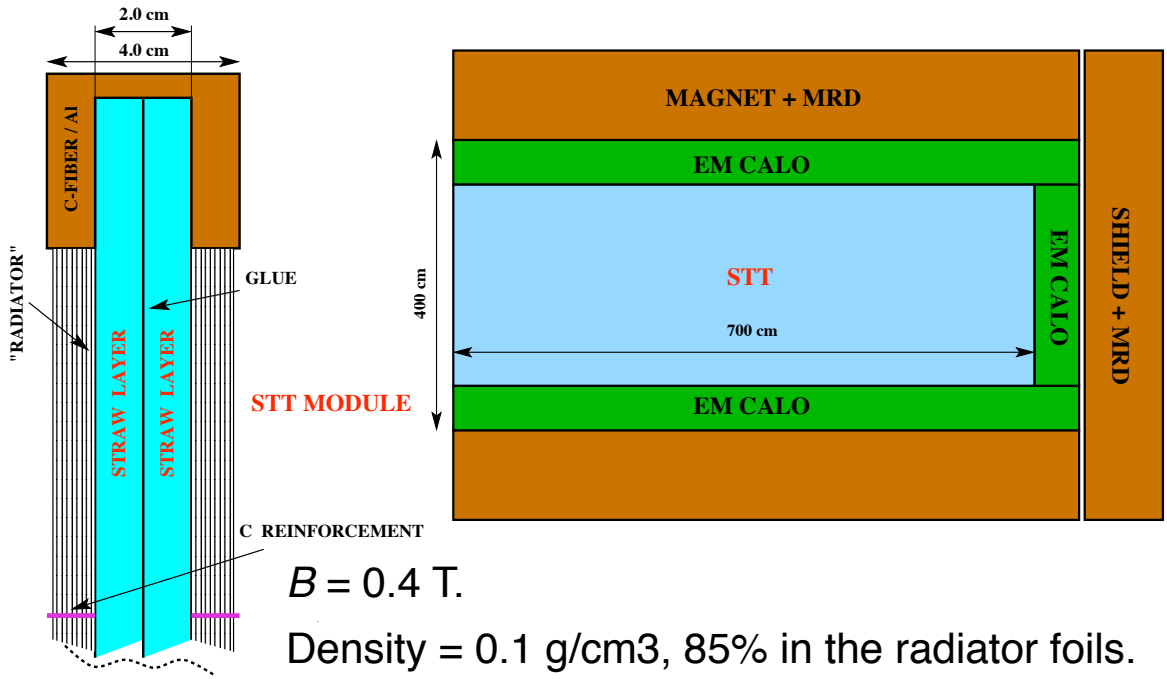

Figure 1: Sketch of the proposed detector showing the inner straw tube tracker (STT), the electromagnetic calorimeter (EM CALO) and the magnet with the muon range detector (MRD). The inernal magnetic volume is $\mathbf{4.5}\boldsymbol{m} \times \mathbf{4.5}\boldsymbol{m} \times \mathbf{8}\boldsymbol{m}$. Also shown is one module of the proposed straw tube tracker (STT). Two planes of straw tubes are glued together and held by an Al-frame. In front of each module a plastic radiator made of many thin foils provides 85% of the total mass of the detector and can be adjusted according to the required resolution and statistics. The module design is taken from the COMPASS experiment.

containing a double straw layer - as shown in Figurefig-det-schematic. We plan to have readout at both ends of the straws to resolve ambiguities in the hit assignment. In front of each module, plastic foils, the "radiators", provide 85% of the mass and allow a measurement of the transition radiation (TR) which will yield continuous identification of electrons though the tracking volume. Much of active target is composed of carbon. We propose to use Xe-gas in the straw tubes (Xe/CO_2) to maximize the TR capability. Finally we shall measure dE/dx enabling the identification of protons, charged pions and kaons. The identification of individual tracks as protons is especially important for the neutrino Quasi-Elastic (QE) and resonance ($\boldsymbol{\Delta}$) interactions.

(2) Possibly Full Electromagnetic Carolimeter Coverage: The tracking volume will be surrounded by an electromagnetic calorimeter (ECAL) on the four sides and at the downstream end. The ECAL will have transverse and longitudinal segmentation. The default design of ECAL calls for a lead-scintillator calorimeter. In the first stage of construction, we propose to construct ***only*** the downstream end of the ECAL and the last 2 m of the sides, as we learn from detailed simulation. Later, we hope to instrument completely the sides making the ND fully hermetic. (The granularity will be decided after detailed calculations.)

(3) Improved Muon-Identification: We propose to tag 95% of the emergent muon in the $\boldsymbol{\nu_\mu}$-CC sample in contarst with the 85% efficiency in NOMAD. The sides of the dipole magnet will be instrumented with muon-range detector (MRD). Instrumentation in the magnet yoke and the muon detector coverage outside the magnet will enable this improvement (see Figure 2). The muon

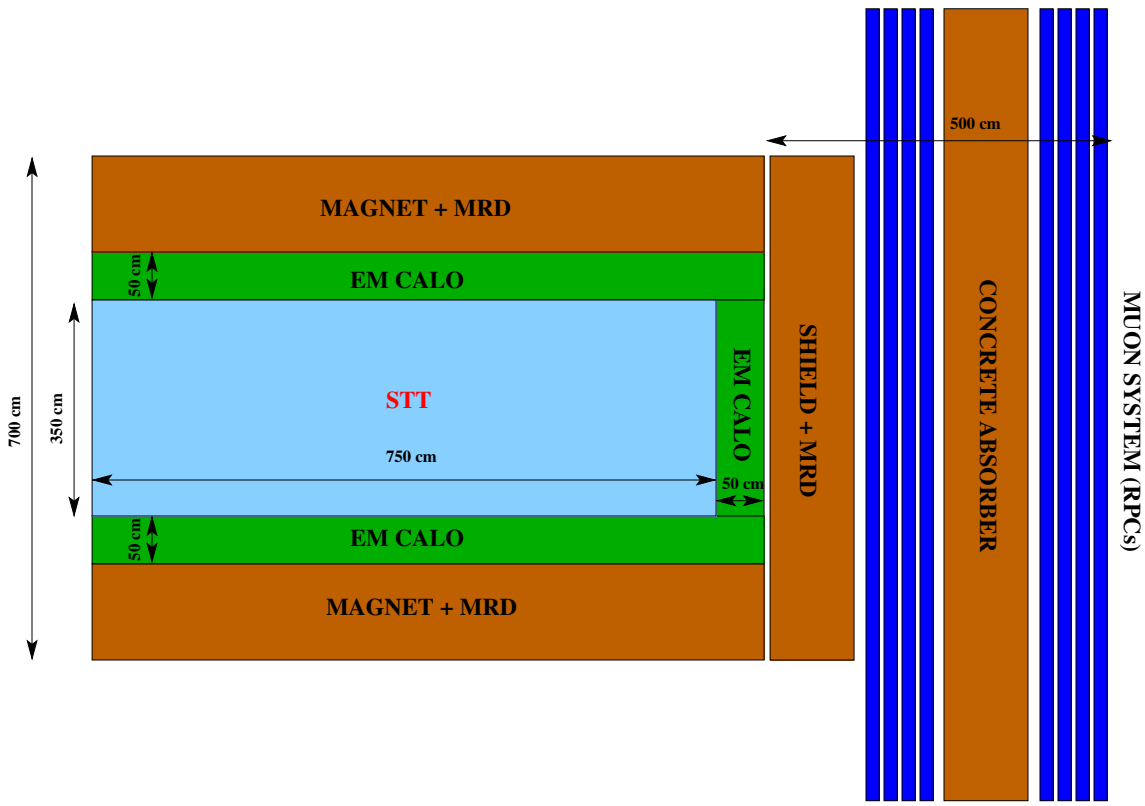

Figure 2: Layout of the HiResMnu with external muon detectors.

detectors will be inexpensive RPC's. The muon detector is only meant to provide the identification of the muon — the muon momentum itself will be measured by the STT inside the B-field.
(4) Trigger: Unlike NOMAD, the trigger will not be based upon the geometry or charge-bias. We aim to have $\approx$ 100% trigger efficiency for any event with $\geq$ **100** MeV of visible energy in the tracker or ECAL.

3 Expected Detector Performance

We expect that the space point resolution of the STT will be $\mathbf{200\mu}$ on individual hits with a time-resolution of about 1 nanosecond. Both the test-beam measurements of the ATLAS-TRT and COMPASS-STT have achieved a better than 170μ resolution. The resolution of the coordinates of a ν_μ-CC event, , $\mathbf{\Delta(X,Y,Z)}$, is expected be $\mathcal{O}(\mathbf{100\mu})$, a value commensurate with the space point precision and the NOMAD experience. Figure 4 shows the longitudinal (Z-position of the ν-vertex) radiography of NOMAD revealing the elements of the tracker such as the Kevlar skin, the Honeycomb, and the Gas-gap within the tracking drift-chambers. The STT will afford a better vertex resolution by a factor of two, or more, than that of NOMAD.

The energy resolution of the proposed ECAL will be $\approx \mathbf{6\%/\sqrt{E}}$ and a time resolution of 1 ns for e/γ with energy $\geq \mathbf{100}MeV$. The muon detector, composed of RPC's, will have a space point resolution of about 200μ and a time resolution of a few nano seconds. The MRD in the magnet will permit a muon-ID down to 200MeV. The momentum resolution of a $\nu_\mu(\bar{\nu}_\mu)$-CC induced μ^-

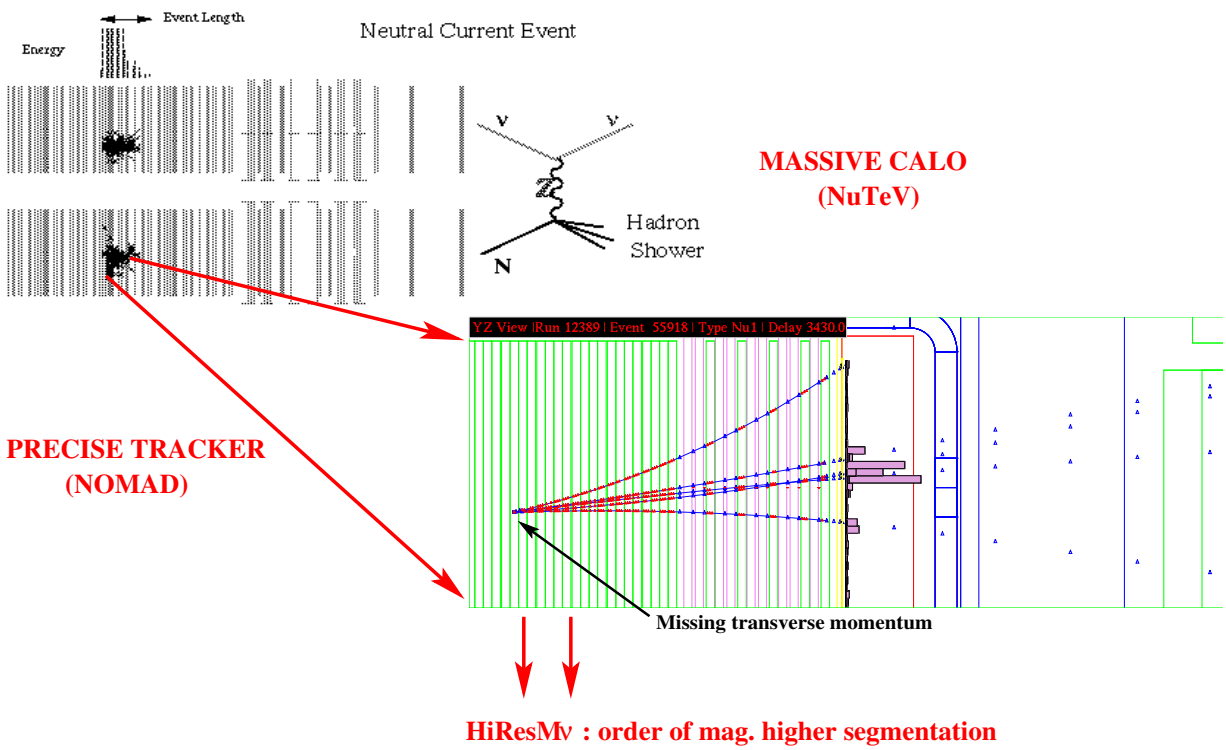

Figure 3: Candidate NC Event in NuTeV and NOMAD. In tracking charged particles HiResMν will provide a factor of two higher segmentation along z-axis and a factor of six higher segmentation in the transverse-plane compared to NOMAD.

(μ^+) is shown in Figure 5 for a 2m long track. It should be noted that the average length of a μ^- (μ^+) from a CC is about 3.5m. The energy resolution of a $\nu_e(\overline{\nu_e})$-CC induced e^- (e^+) is also shown in the Figure 5 where the electronic charge and direction are measured in the STT and the energy in the ECAL.

A HiResMnu-type ND will measure all **four** neutrino species: the easily identified ν_μ- and $\overline{\nu}_\mu$-CC events with $\geq$ **90%** efficiency, and the more challenging ν_e- and $\overline{\nu}_e$-CC with $\geq$ **50%** efficiency with a systematic precision $<<$ **1%**. Figure 6 shows a ν_μ-CC event in NOMAD, the $\mu^\pm$ being easily measured in the tracker with a B-field. The novel feature of a low density detector is a clear measurement of the charged- and neutral-hadrons composing the accompanying hadronic-jet. Figure 7 shows a $\overline{\nu}_e$-CC event, the most difficult of the ν-species to measure, in NOMAD; the e^+ is identified by the curvature, the dotted lines show the bremsstrahlung photons associated with the e^+-track, the charged- and neutral-hadrons are also identified. The proposed experiment will have substantially better resolution than NOMAD. The bottom line is that HiResMν will accurately determine the relative content and E_ν spectrum of all all four ν's.

We have conducted simulations of the proposed HiResMnu detector to study the sensitivity to the following processes: (a) ν_e-CC, (b) absolute ν-flux measurement using ν-electron elastic neutral and charged (inverse muon decay) current scattering, (c) π^0 and γ reconstruction in NC, (d) ν_μ-QE, and (e) the shape of the ν_μ and $\bar{\nu}_\mu$ flux as a function of E_ν. The detector simulation is based on a parameterized response of particles. The NOMAD data serve as invaluable calibration for these studies. For each calculation, we conduct an identical simulation using the NOMAD-

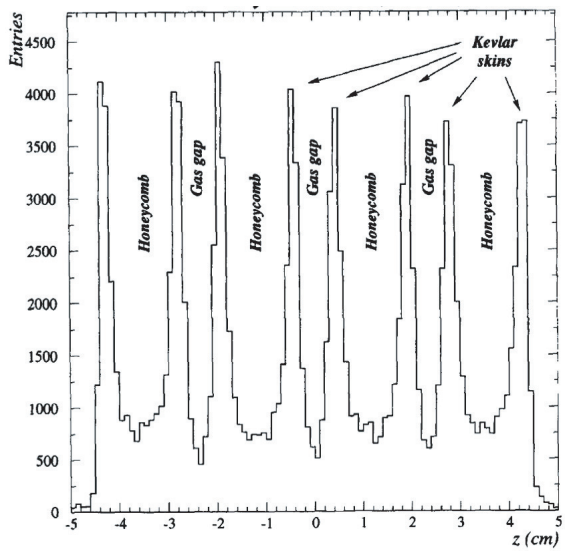

Figure 4: A neutrino radiograph of the NOMAD drift chambers shows the internal structure of the tracking volume. It illustrates the high resolution of the z-postion of the vertex.

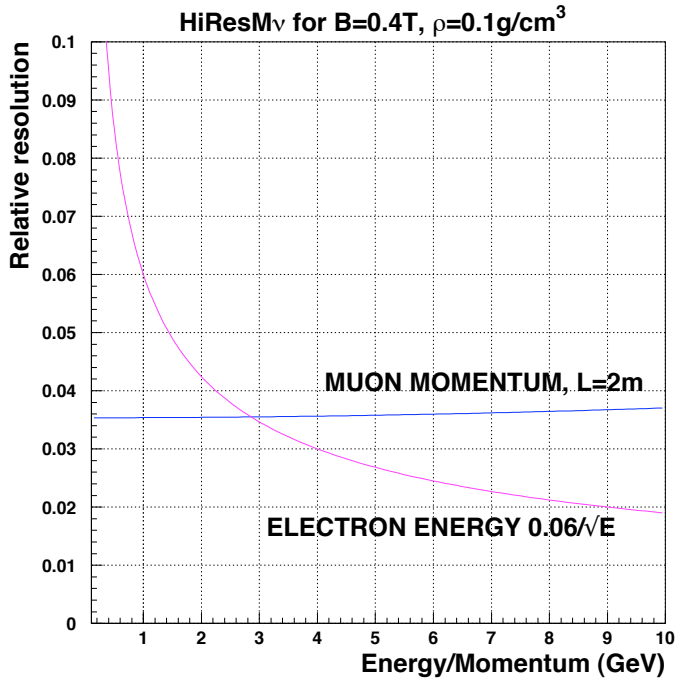

Figure 5: Momentum resolution of a $\nu_\mu(\bar{\nu}_\mu)$-CC induced μ^- (μ^+) is shown, in blue, as a function of the muon momentum. Also shown, in red, is the resolution of $\nu_e(\overline{\nu_e})$-CC induced e^- (e^+).

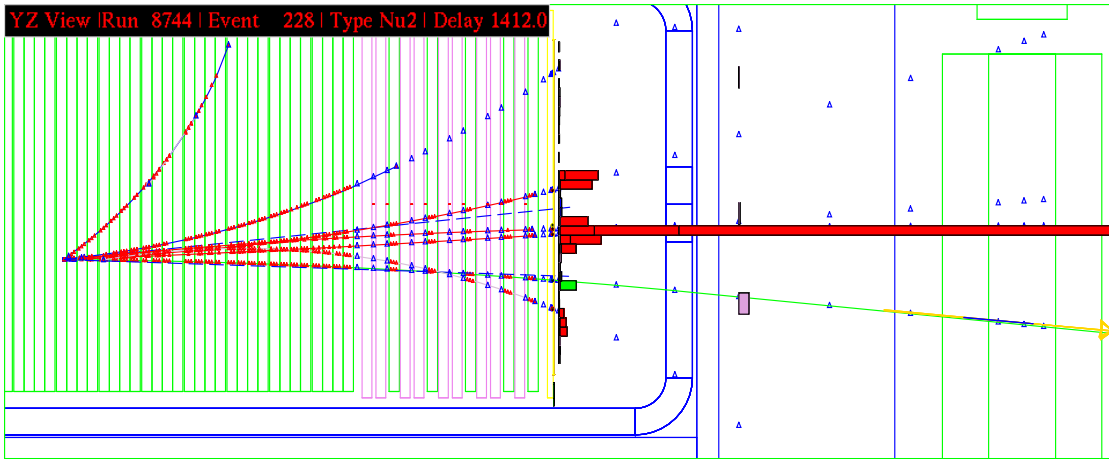

Figure 6: A ν_μ CC Event Candidate in NOMAD. The HiResMnu will have more sampling points and better muon coverage.

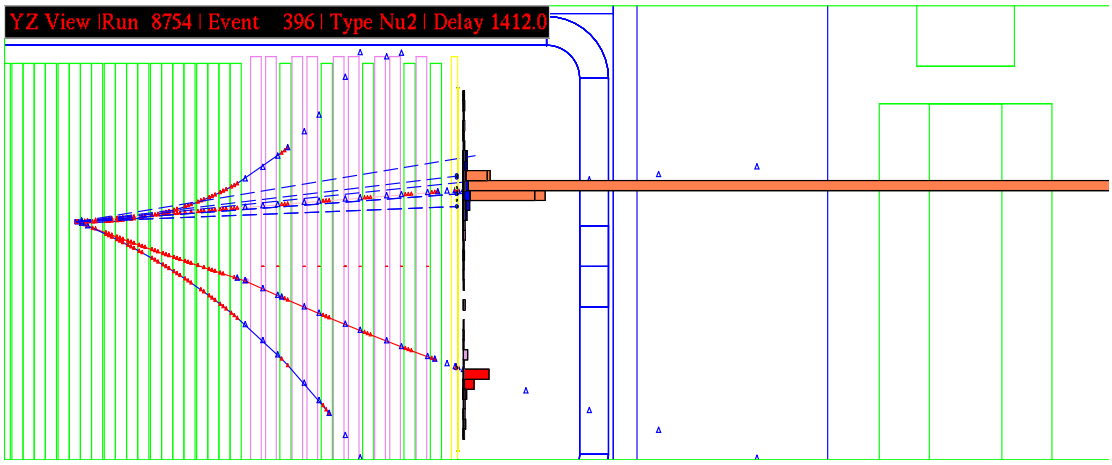

Figure 7: A $\bar{\nu}_e$ CC Event Candidate in NOMAD. The positron track with bremsstrahlung photons are clearly visible. The HiResMnu will have more sampling points, TR, and and better γ acceptance.

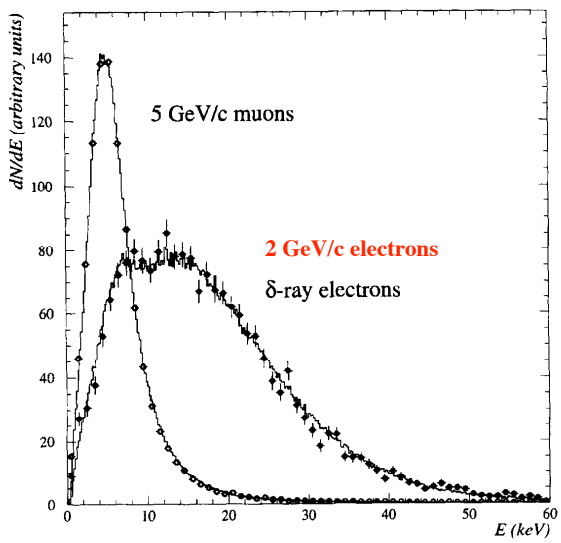

Figure 8: Comparison of the TR of a 5 GeV muon and a 2 GeV electron.

parameters and checked the results against the NOMAD data and Geant-based MC. Typically, the results agree to within $\pm 15\%$. In the following we summarize these sensitivity studies.

3.1 Sensitivity to ν_e-CC

The goal of this study is to determine the efficiency of $\nu_e(\overline{\nu_e})$-CC signal and the reduction of the much larger NC and ν_μ-CC samples, i.e. the purity. The relative abundance of ν_μ-CC:NC:nu_e-CC is about 1:0.35:0.01. The ν_e-CC analysis proceeds in two steps.

In the first step, we require that there be a negatively charged particle consistent with the electron-TR identification in the event. Figure 8 compares the TR for a 5 GeV muon with a 2 GeV electron as measured by the NOMAD TR-subdetector. Figure 9 shows the electron TR-efficiency as a function of electron momentum for a 10^{-3} rejection of charged pions. Geant simulation of proposed STT confirms these efficiencies for a 1/1000 pion-rejection. (See **DocDB#432-v1**). The surviving background events are completely dominated by an asymmetric photon conversion, producing an actual e-/e+, near the event vertex.

In the second step, we require that the TR-identified electron be kinematically isolated from the hadronic jet. An outstanding feature of HiResMnu is the measurement of the momentum vectors in the plane transverse to the ν-direction. Event-by-event determination of the missing transverse-momentum (P_T^m) vectors offers a powerful tool to constrain the event kinematics, and helps distinguish the NC from CC events, especially when the leading lepton from CC evades detection. Figure 10 shows the kinematic variables accessible in HiResMν. The P_T^m-vector measurement allows a clean separation of NC (non-prompt) from CC (prompt) events. To isolate the ν_e-CC induced prompt-e^- from the NC-induced photon-conversion, we use a multivariate likelihood function built using the momentum vector information of the lepton and the hadron. A mild cut on the lepton versus hadron isolation diminishes the signal efficiency by 10% while reducing the background by 80%. The final efficiency (55% average) and the purity (96% average) of the ν_e-CC is shown in Figure 11 as a function of the ν_e-energy. The $\overline{\nu_e}$-CC analysis is conducted in a similar fashion. For the $\overline{\nu_e}$-CC, if we choose to keep the average efficiency at 50% then the average

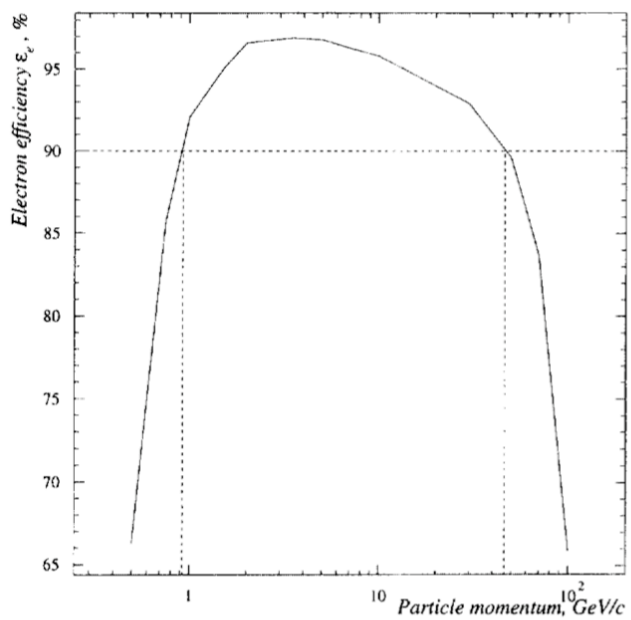

Figure 9: Electron TR-ID Efficiency as function of the electron momentum for a 1/1000 rejection of pions.

purity will be 88%.

3.2 Sensitivity to the Absolute ν Flux Measurement

The proposed ND will offer an ***in situ*** absolute ν flux measurement using (a) ν-electron neutral current elastic scattering with an accuracy of $\approx \mathbf{2.5\%}$ for $E_\nu \leq \mathbf{10}$ GeV; (b) ν_μ-electron charged current scattering with an accuracy of $\approx \mathbf{3\%}$ for $E_\nu \geq \mathbf{11}$ GeV (average-E_ν $\approx$25 GeV); and (c) the slope of $d\sigma(\nu_\mu - QE)/dQ^2$ on a deuterated target. The three methods are systematically independent. We have studied the first two methods and summarize our findings; the feasibility of the last method is being investigated.

3.2.1 Absolute ν Flux using ν-Electron Elastic NC Scattering

Using the precise measurement of the weak mixing angle at the Z^0-pole, the standard model can predict the cross-section of the ν-electron elastic neutral current scattering, $\nu + e^- \rightarrow \nu + e^-$ (NuElas), with $\approx \pm\mathbf{1\%}$ accuracy at the LBNE energies. Therefore, if we could detect NuElas and accurately constrain the background then we can use the SM cross-section to measure the absolute ν-flux. It should be noted that 91% of the LBNE-ν's are ν_μ in the focus-positive mode.

The NuElas will produce a single e^- collinear with the ν-beam ($\leq$ **40** mrad). The background, dominated by the asymmetric conversion of a photon in an ordinary ν-N neutral current event, will produce e^- and e^+ in equal measure with much broader angular distribution. The key to this measurement is measuring the angle, energy, and charge of the electron or positron: these are the strength of the HiResMnu design. The analysis requires a single e^- or e^+ passing the TR-ID and requires that 'forwardness' variable, $\zeta = P_e(1 - \cos\Theta_e) \leq 10^{-3}$. Figure 12 presents a comparison of the angular distributions of NuElas signal (symbol) with those of the hadronic background (histos) where a single charged track is reconstructed. The figure shows that the

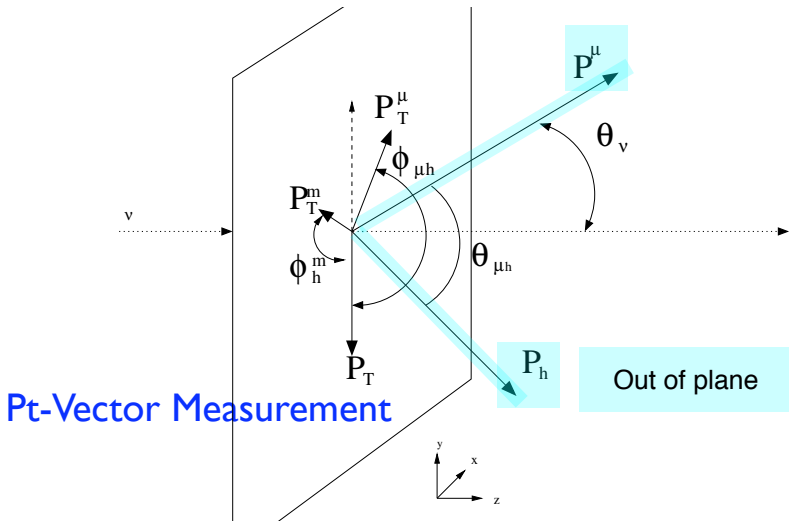

Figure 10: Reconstruction of the event kinematics from individual tracks and neutral clusters in the ECAL is a powerful tool to discriminate NC from CC events.

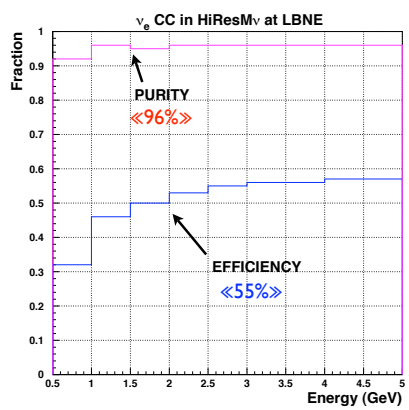

Figure 11: Efficiency and purity of the ν_e-CC sample as a function of the ν_e-energy

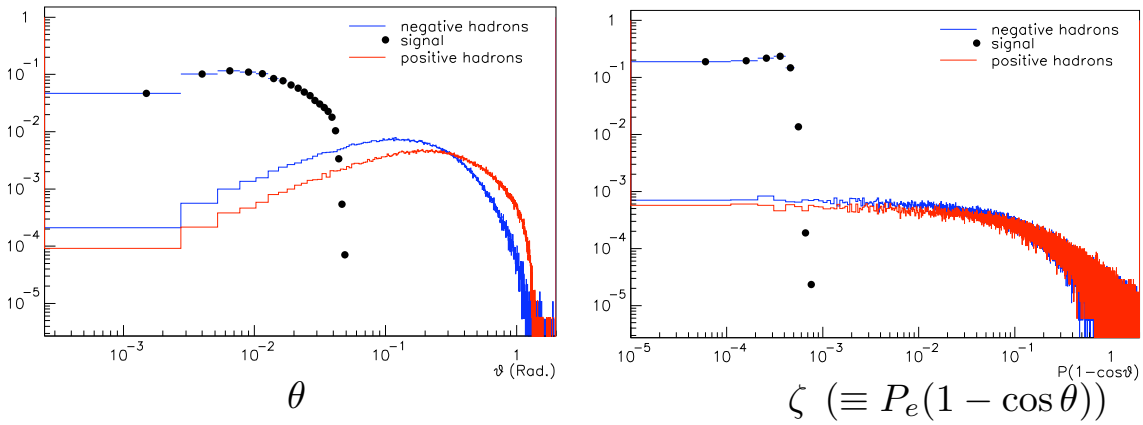

Figure 12: Comparison of Θ and ζ distributions of NuElas signal and background.

background is benign. The efficiency of the signal is about 64% with a $\mathbf{10^6}$ reduction of the background. The background, though small, is symmetric in charge. Thus it will be measured in the detector. The measurement of NuElas will be dominated by the statistical error. We estimate that the absolute flux of the LBNE neutrinos can be determined to a $\leq \mathbf{2.5\%}$ precision. Having measured the momentum and angle of the signal electron, the incident neutrino energy can be calculated. Figure 13 contrasts the E_ν distribution derived from P_e, Θ_e with the incident E_ν. The figure shows that in the $E_\nu \leq \mathbf{5}$ GeV range the shape of the ν-spectrum can also be determined using the NuElas.

3.2.2 Absolute ν Flux using Inverse Muon Decay

The ν_μ-e^- CC interaction, the inverse muon decay, $\nu_\mu + e^- \rightarrow \mu^- + \nu_e$, offers an elegant way to determine the absolute flux. Given the m_μ-threshold, IMD, however, requires a minimum $E_\nu \geq \mathbf{10.8}$ GeV. Over a three year period, the HiResMnu detector should see $\geq \mathbf{1000}$ IMD events. The reconstruction efficiency of the single, energetic, and extremely forward ($\zeta_\mu << 10^{-3}$) μ^- is $\geq \mathbf{98\%}$. The angular resolution of the IMD-μ is $\leq \mathbf{1}$ mrad. The background, primarily from the ν_μ-QE, is negligible — and will be precisely measured. We anticipate that the IMD events will allows the absolute flux at high energies to be determined to $\approx \mathbf{3\%}$ precision.

3.3 Sensitivity to the π^0, γ, and $\pi^\pm$ Identification

The principal background to the ν_e- and $\overline{\nu}_e$-appearance comes from the NC-events dominated by π^0's. The proposed ND is designed to measure π^0's with high accuracy in three topology: (i) both photons convert in the tracker ($\simeq \mathbf{25\%}$), (ii) one photon converts in the tracker and the other in the calorimeter ($\simeq \mathbf{50\%}$), and (iii) both photons convert in the calorimeter. The first two topologies afford the best resolution since the tracker provides accurate γ-direction measurement.

What sort of photon reconstruction resolution do we expect in the proposed detector? Figure 14 and Figure 15 display the exclusive two photon events in NOMAD. Figures demonstrate the ability to reconstruct low-energy photons in a detector with $\rho = 0.1 gm/cm^3$. The proposed detector is designed to have substantially improved photon reconstruction ability in STT down to 80 MeV.

To estimate the π^0 reconstruction efficiency, we focussed on events where at least one photon

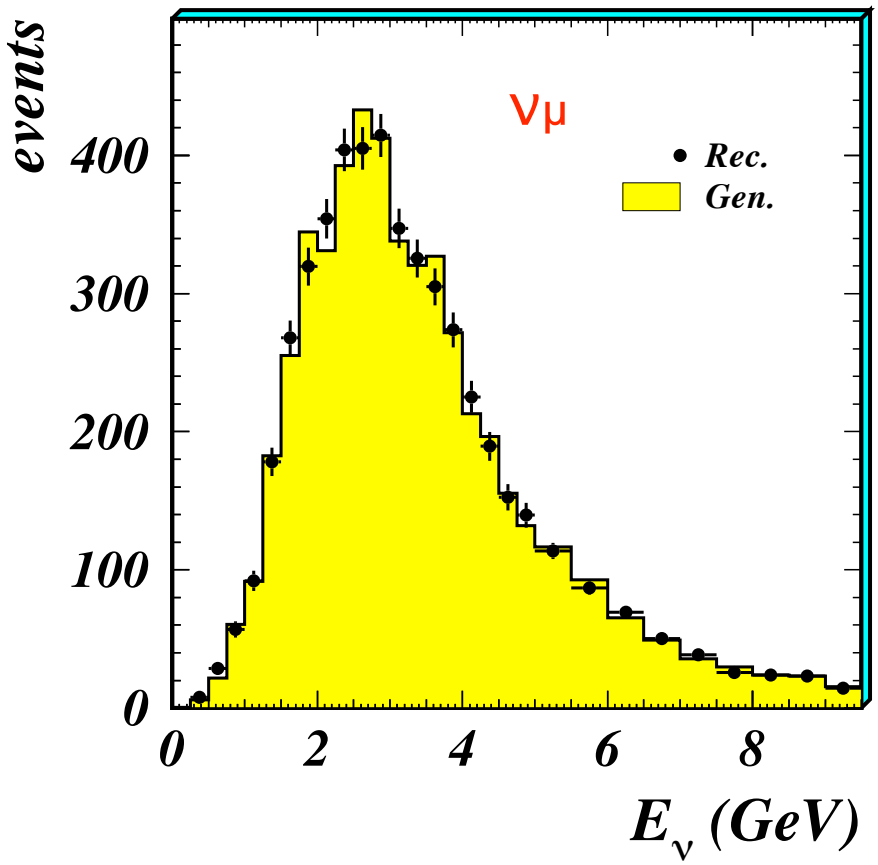

Figure 13: Comparison of derived E_ν using the reconstructed momentum and angle of the electron and the incident E_ν (histo).

converts in the STT. Figure 16 shows the π^0 reconstruction efficiency as a function of π^0 energy in NC events. If we include photons that reach the ECAL, the reconstruction efficiency is expected to be $\geq$ **75%**. Figure 17 shows the invariant mass distribution of the reconstructed photons in the ν_μ-CC sample of NOMAD; Figure 18 shows the reconstructed photons in the NC sample of NOMAD. Improvements in the π^0 reconstruction in HiResMν comes from two considerations: first, 50% more photons will convert in the tracker; second, the e^-/e^+ track will have a factor of 12 more track points than that in NOMAD enabling more efficient reconstruction of low momenta e^- and e^+. Finally the combinatorial background will be much smaller in LBNE than NOMAD.

The discussion above also implies that the reconstruction of events with exclusive single photon will be straight forward. Exclusive photon events occur rarely since to the first order photons appear in pairs, from π^0-decay, in ν-interactions. If processes exist that produce single photons, then 50% of these will be cleanly reconstructed in HiResMnu. Figure 19 shows NOMAD events where a single photon was reconstructed. The proposed detector will have better resolution to reconstruct γ's than NOMAD and will completely determine the ν_μ-CC- and ν-NC-induced photons, exclusive and semi-exclusive, as a function of E_{Vis} and angle with high purity. By contrasting the π^0 mass in the tracker versus in the calorimeter, the relative efficiencies of photon reconstruction will be well constrained.

Finally, the $\pi^\pm$ will be measured by the tracker including the dE/dx information. An *in*

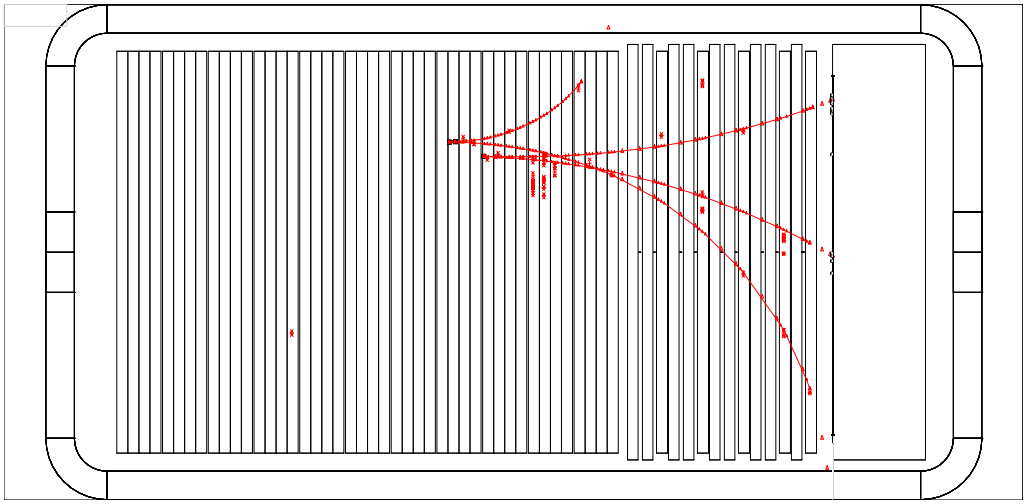

Figure 14: An exclusive two-photon event in NOMAD.

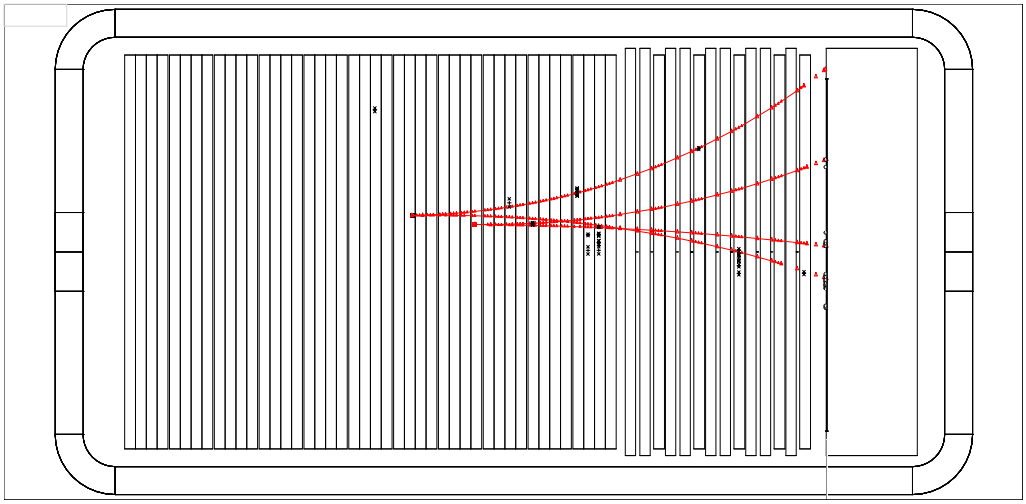

Figure 15: Another exclusive two-photon event in NOMAD.

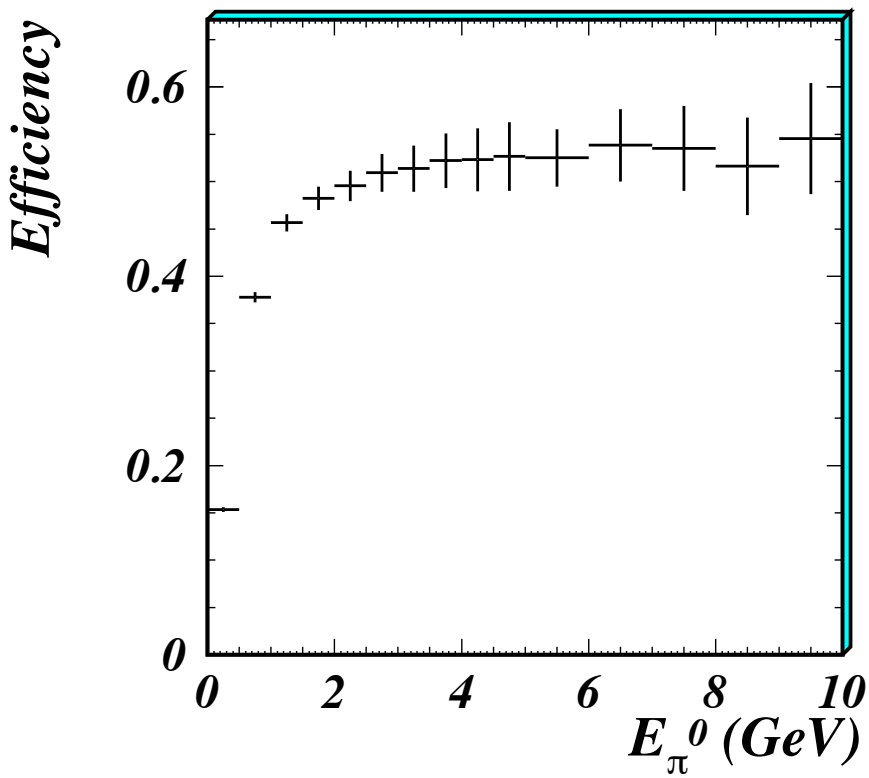

Figure 16: π^0 reconstruction efficiency as a function of π^0 energy in NC events.

situ determination of the charged pions in the $\nu_\mu(\overline{\nu}_\mu)$-CC — with μID and ***without*** μID —, and ν-NC is crucial to constrain the systematic error associated with the $\nu_\mu(\overline{\nu}_\mu)$-disappearance, especially at low-E_ν. The HiResMν determination of the charged pion production in non-μID-CC and NC will all but eliminate this error. The NOMAD event pictures of ν_μ-CC, $\overline{\nu}_e$-CC and NC show that the measurement of the charged hadrons in HiResMν will be a routine task.

3.4 Sensitivity to ν_μ-QE

In the LBNE physics program, the quasi-elastic (QE) interactions are special. First, the QE cross-section is substantial because the energy is low. Second, a measurement of ν_μ-QE provides, to first oder, a direct measurement of flux. Third, because of the simple topology — a μ^- and a proton —, the interaction provides direct constraints on Fermi-motion and final state interaction (FSI) dynamics. The key to ν_μ-QE is to measure the two-track ($\mu^- p$) topology. The experimental challenge is the reconstruction of the emergent proton. Figure 20 and Figure 21 show ν_μ-QE candidate events in NOMAD. The HiResMnu is designed to accurately and efficiently identify the proton and measure its momentum vector. The STT will have the ability to measure the "dE/dx" of the recoil proton. The efficiency of reconstructing the proton will be twice that of NOMAD. By contrasting the 2-track topology with 1-track (which is what most experiments measure), one can obtain an ***in situ*** measure of the Fermi-motion. Furthermore, the two topologies are very sensitive to the FSI parameters. By demanding consistency in the cross-section between the two topologies we will empirically constrain the nuclear motion and the FSI parameters. Figure 22

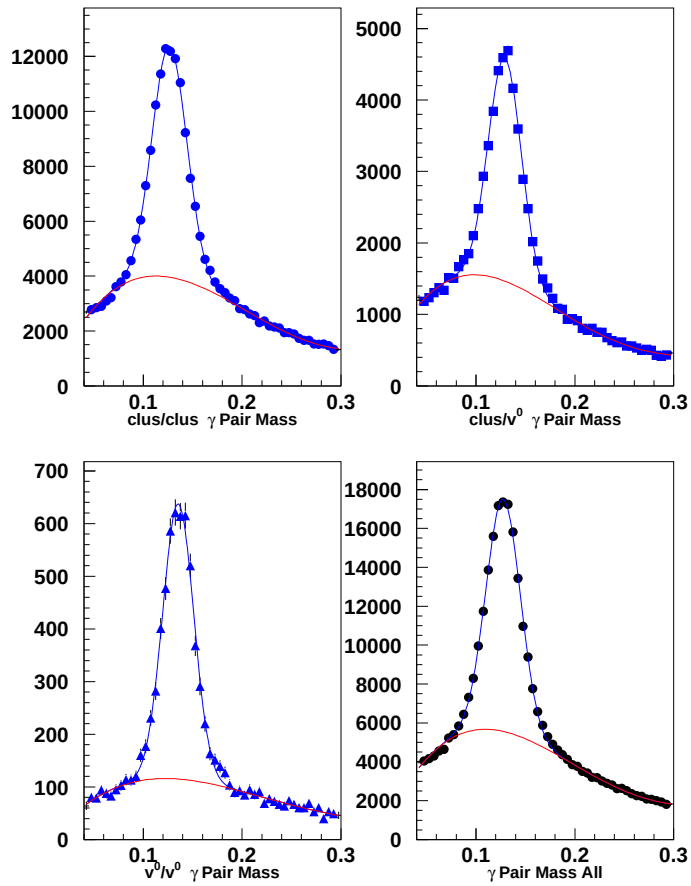

Figure 17: Reconstruction of π^0 in inclusive ν_μ-CC events in NOMAD (preliminary).

shows the efficiency and purity of reconstructing ν_μ-QE induced $\mu^- p$ events as a function of E_ν in LBNE.

3.5 The ν_μ and $\overline{\nu_\mu}$ Flux as a Function of E_ν and FD/ND Prediction

The most promising method to determine the shape of the ν_μ and $\bar{\nu}_\mu$ flux is by measuring the low-ehadronic (ν) CC events — the low-ν^0 method of relative flux determination [11]. In this analysis, the key measurable quantities are the resolution for low-ν events and the systematic precision of the muon-momentum. The $\nu_\mu(\bar{\nu}_\mu)$-CC flux provides a measure of the $\pi^+/K^+/\mu^+$ ($\pi^-/K^-/\mu^-$) content of the beam. Following the NOMAD analysis we first obtain the relative $\nu_\mu(\bar{\nu}_\mu)$-flux at ND. Next, we fit the $d^2\sigma/dx_F dP_T^2$ of the parent mesons to the ν_μ-flux. The ingredients to the empirical fit to the meson production cross-section (EP) are the measured ν_μ-flux at ND, constraints from the hadro-production experiments (MIPP), and the simulation of the beam transport. The systematic-error analysis includes ν^0-correction, composition of CC (QE .vs. Resonance .vs. transition-region .vs. DIS), muon-energy scale, low-hadronic energy resolution, beam-trasport errors and different functional forms. Figure 23 shows the mock-data and the fitted flux at ND positioned 1000m from the target. Having constrained the $d^2\sigma/dx_F dP_T^2$ of the pions/kaons, one can predict the flux at FD. Figure 23 also shows the true versus the fitted

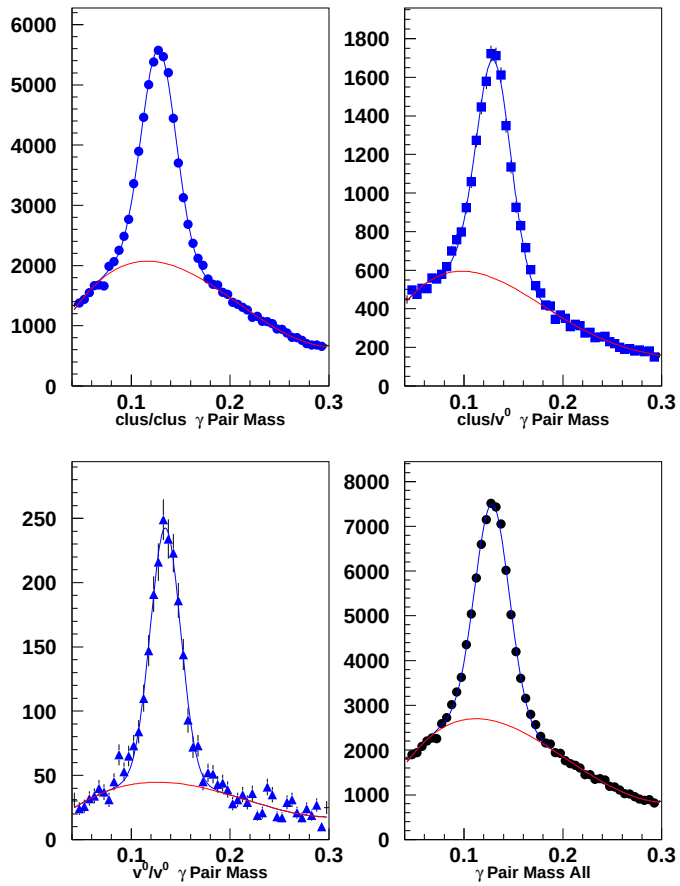

Figure 18: Reconstruction of π^0 in inclusive NC events in NOMAD (preliminary).

FD/ND ratio. (The calculation presented here has poor statistics for $E_\nu \geq 20$ GeV; so we will focus mostly on the $E_\nu \leq 20$ GeV region.) The figure shows that the fitted FD/ND agrees with the true value to within 2%. Figure 24 shows the $\bar{\nu}_\mu$ results. We repeated the study for ND at 500m, 750m, 1500m, and 2000m. There are obvious advantages to ND being closer to the target region. Figure 25 and Figure 26 show the results for the relative flux and FD/ND determination when ND is at 500m. We have two preliminary conclusions: first, that the high resolution detector will reliably predict the FD/ND to $\leq 2\%$ precision as a function of E_ν; second, an ND at 500m can predict the FD/ND flux just as precisely as an ND at 1000m.

We point out that an accurate measure of ν_μ-, $\overline{\nu}_\mu$-, and $\overline{\nu}_e$-CC provides an absolute prediction of the ν_e-content of the beam. The reason is that ν_μ-($\overline{\nu}_\mu$-) CC-spectrum provides a measure of the $\pi^+/K^+/\mu^+$ ($\pi^-/K^-/\mu^-$) content of the beam, and the $\overline{\nu}_e$-CC provides a direct measure of the elusive K^0_L, the sources of ν_e.

We have charted out a composite program of measurement of the LBNE ν-flux with a HiResMnu-type ND. The program includes an absolute flux determination using ν-electron neutral and charged current interaction. The ultimate precision on the absolute flux will be $\leq 2\%$ The ND will measure the ν_μ, $\bar{\nu}_\mu$, ν_e, and $\overline{\nu_e}$ CC-spectra. Using the low-ν^0 flux technique and the empirical parametrization of the $\pi^\pm$, $K^\pm$, K^0, and $\mu^\pm$, one can predict the FD/ND ν_μ ($\bar{\nu}_\mu$) flux ratio with $\leq 2\%$ precision in E_ν bins.

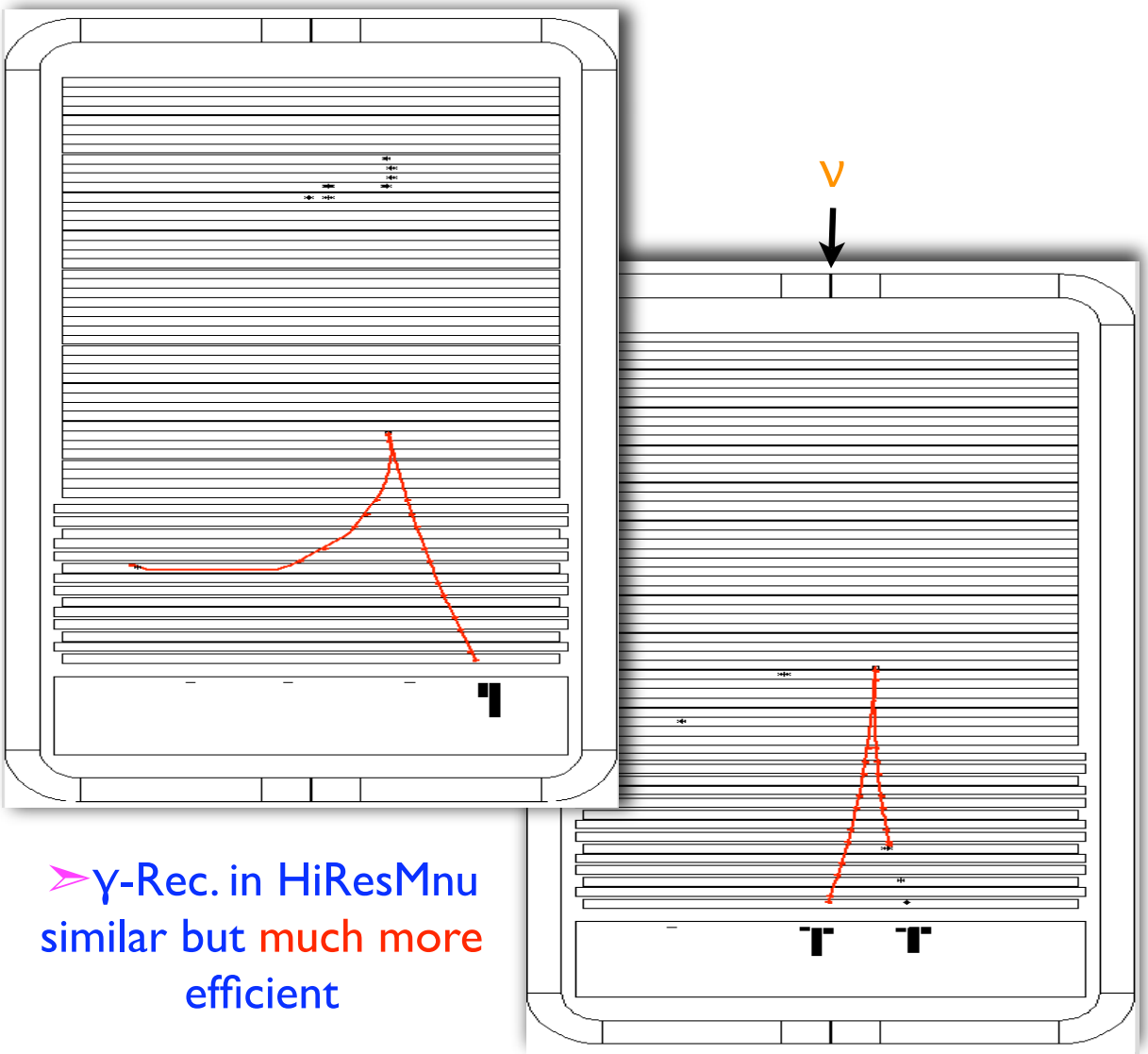

Figure 19: NOMAD events with a single visible photon

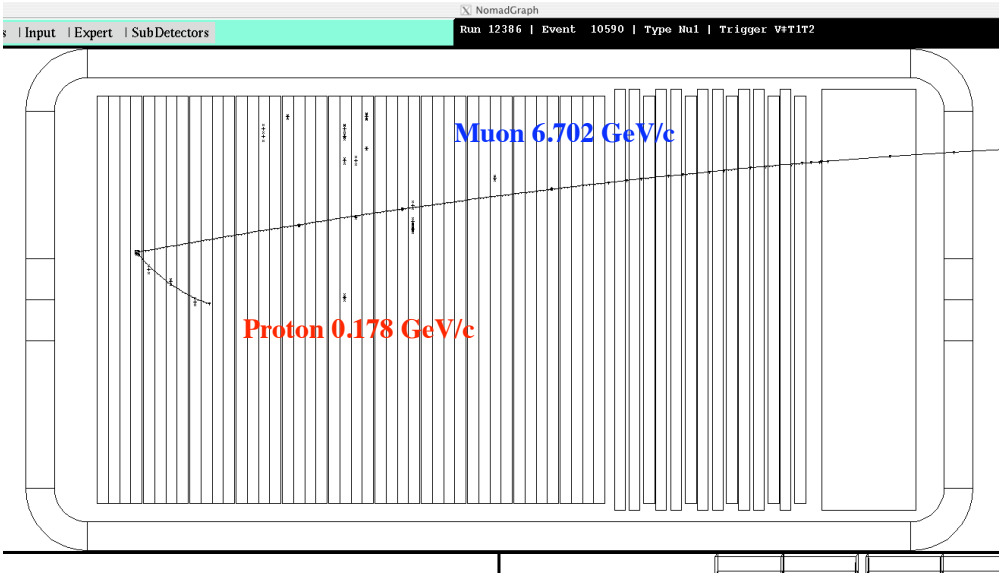

Figure 20: A ν_μ-QE candidate in NOMAD

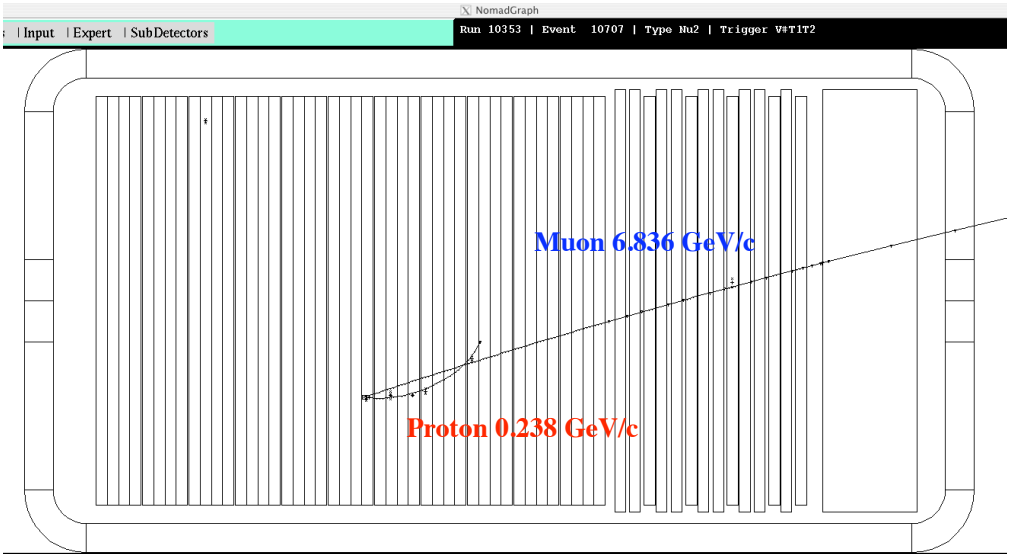

Figure 21: A ν_μ-QE candidate in NOMAD

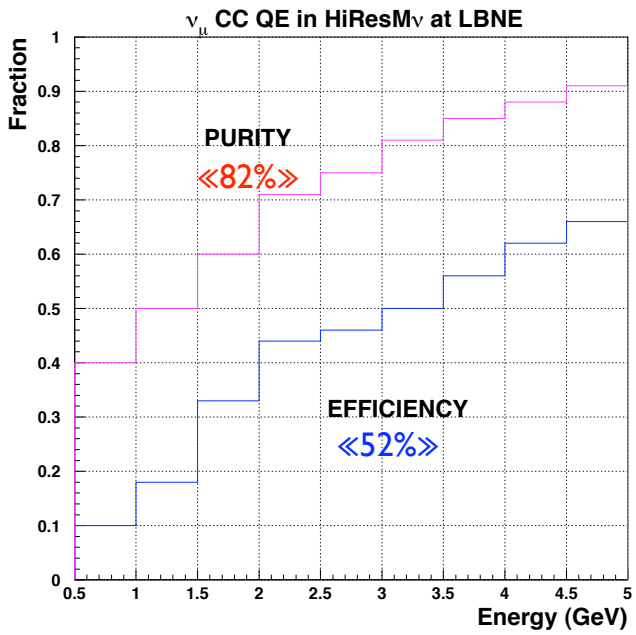

Figure 22: The efficiency and purity of ν_μ-QE induced $\mu^- p$ topology in HiResMnu.

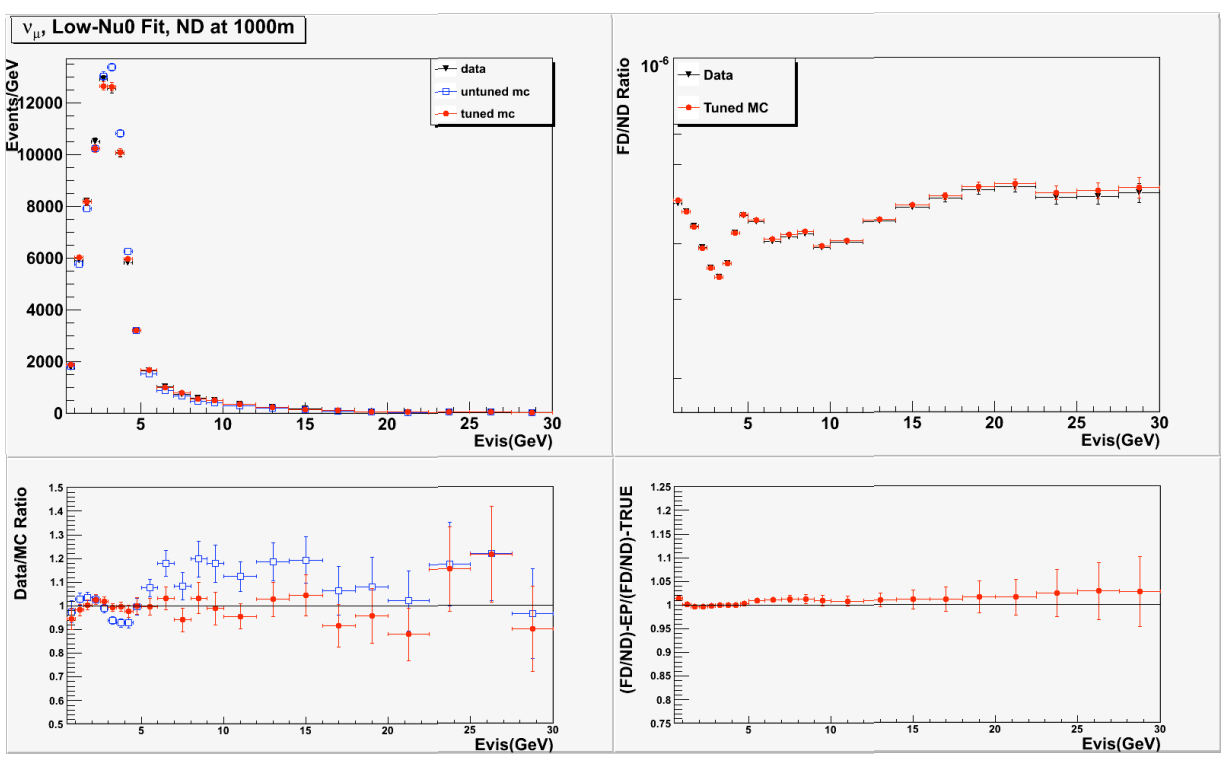

Figure 23: ν_μ flux with ND at 1000m: The 'measured' low-ν^0 and the fitted EP flux at ND (left panels) and the FD/ND comparison.

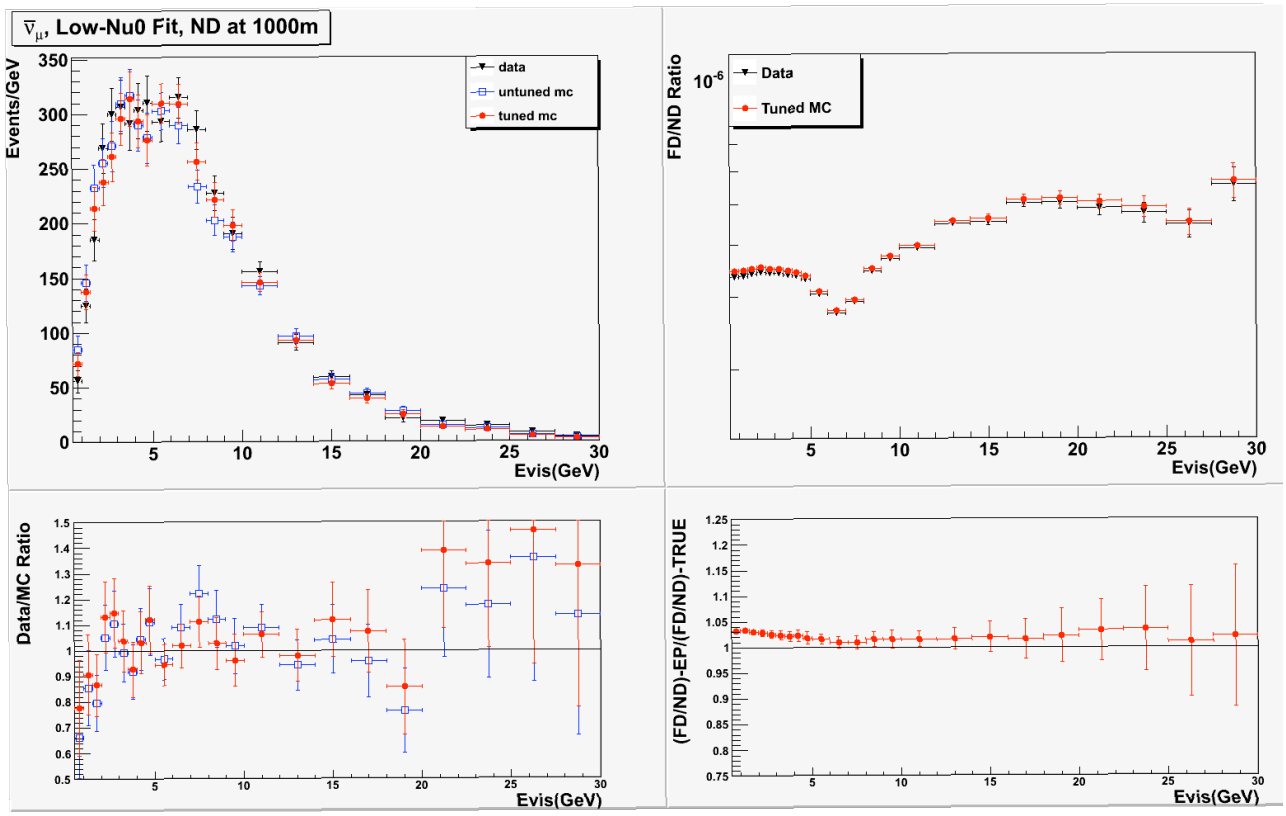

Figure 24: $\bar{\nu}_\mu$ Flux with ND at 1000m: The 'measured' low-ν^0 and the fitted EP flux at ND (left panels) and the FD/ND comparison.

4 ND Hall and Infrastructure Needs

4.1 Dimensions, Mass and Detector Stand

Table 1 summarizes some salient specs of the detector.

Item	Spec
Inner magnetic volume	$\mathbf{4.5 \times 4.5 \times 8}$ m^3
STT	$\mathbf{3.5m \times 3.5m \times 4cm}$ (160 modules)
ECAL	50 cm thick
Thickness of "C"'s and Coils	1.3 m
Muon Range Detector (MRD)	Iron ("C"') of the dipole RPC-instrumented
External Muon Detector	μID for high energy ($\geq$ **2.5** GeV) muons

Table 1: Dimensions of the proposed ND

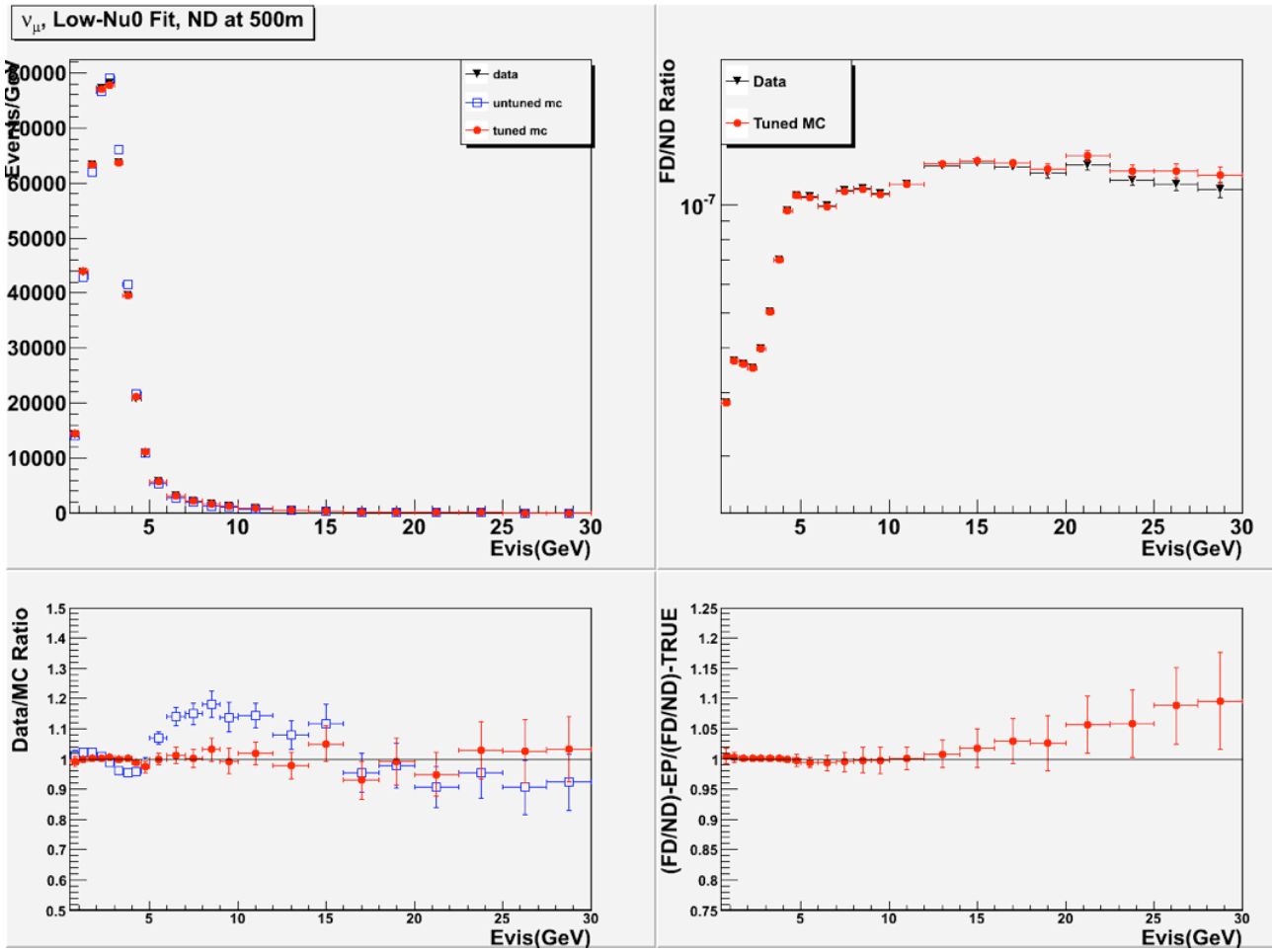

Figure 25: ν_μ flux with ND at 500m: The 'measured' low-ν^0 and the fitted EP flux at ND (left panels) and the FD/ND comparison.

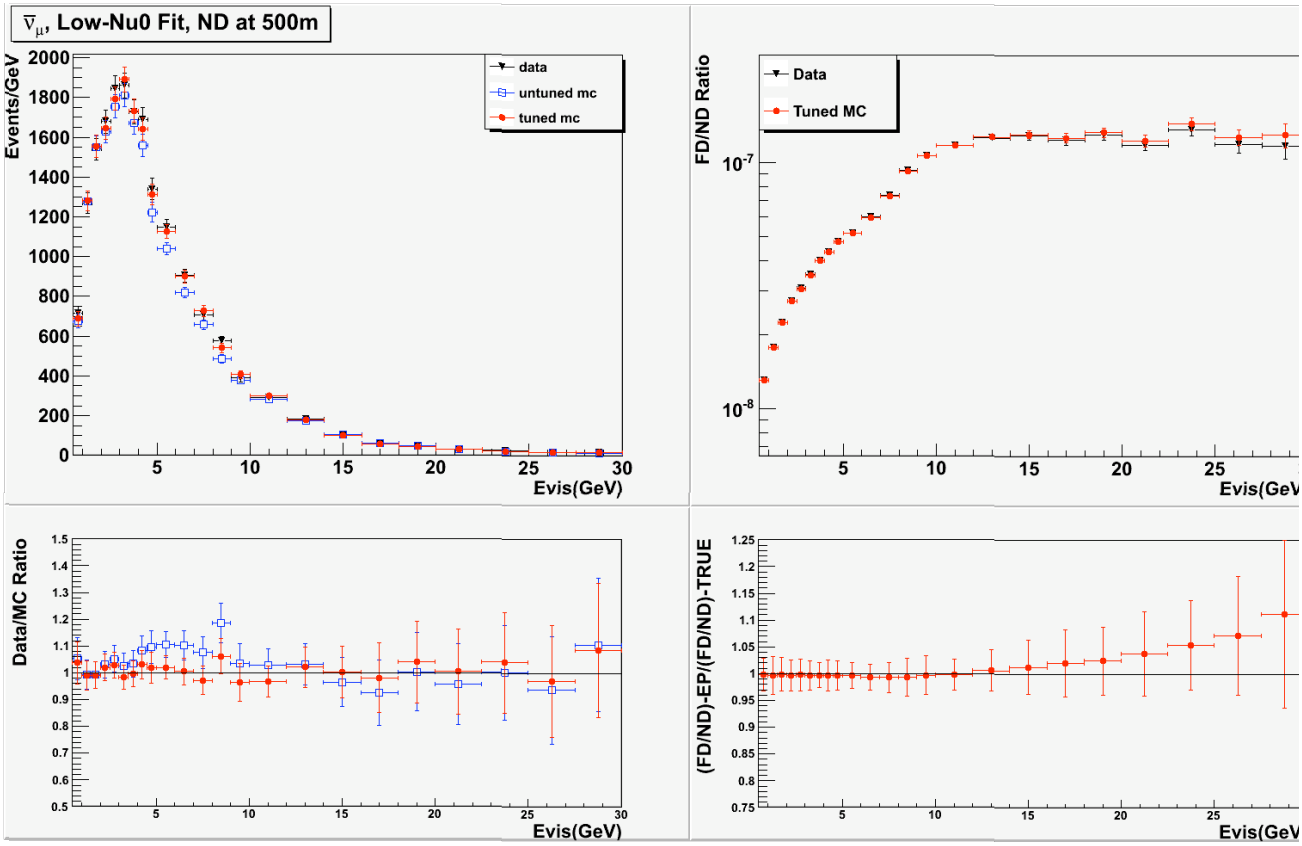

Figure 26: $\bar{\nu}_\mu$ Flux with ND at 500m: The 'measured' low-ν^0 and the fitted EP flux at ND (left panels) and the FD/ND comparison.

4.2 Power Requirement

The main requirement in terms of power consumption comes from the dipole magnet. In order to have a realistic estimate we start from the power required to run the UA1 magnet at a nominal field of 0.4 T, which corresponds to about 1.7 MW. It must be noted that the UA1 magnet was using aluminum coils to minimize the amount of material degrading the energy measurement of jets in hadron collison. However, the HiResMnu does have such a constraint. We plan to use copper coils instead which will lower the power requirements to about 1.04 MW at the nominal field of 0.4 T.

For the STT power consumption we use the numbers measured in the ATLAS TRT detector since the readout chain is essentially the same in HiResMnu and ATLAS. The total number of channels in the ATLAS TRT, including both barrel and end-cap detectors, was about 350,000, for a total power consumption of about 44 kW. In HiResMν we will have 112,640 straws with readout at both ends, giving a total of 225,280 electronic channels and an estimated power consumption of about 28 kW. The ECAL detector is expected to have about 50,000. channels by scaling the corresponding numbers for the T2K ND280 detector. Assuming the same power consumption per channel as the STT this would translate in an additional 6 kW. Finally, for the muon system we estimate a power requirement of about 15 kW.

The total power required to run the HiResMν detector is therefore expected to be about 1.1 MW with the nominal field configuration of 0.4 T. Assuming we run continuously, 365 days/year,

and a nominal cost of the electricity of about \$0.08/kWh the given value of the power consumption will imply an operating cost of about \$771,000./year.

4.3 Cooling Requirement

The cooling of the dipole magnet will require a water flow of about 30 liters/s to dissipate the power produced by the current circulating in the copper coils.

The cooling of the muon system, which is located outside of the magnet, can be achieved by natural convection in the near detector hall. The main cooling requirements are related to the sub-detectors to be installed inside the dipole magnet. To this end, we can use the same cooling system as in the ATLAS end-cap TRT. The STT detector requires an overall $\boldsymbol{CO_2}$ enevelope gas acting as a barrier between the active part of the detector (the straws) and the environment, to prevent the effect of moisture and other souces of pollution. The cooling of the STT detector requires the operation of a dedicated cooling gas system providing $\boldsymbol{CO_2}$ f lows up to $\boldsymbol{100m^3/h}$. Alternately, a standard mono-phase cooling system using a room-temperature $\boldsymbol{C_6F_14}$ fluorinert coolant can be used coupled with heat exchangers on the STT frames and for the front-end electronics boards. The cooling of the ECAL detector can use the same cooling system as the STT.

4.4 Staging Area & Electronics

4.5 Safety Issues

No major safety issues are present for the HiResM$\boldsymbol{\nu}$ detector. All gases used are non-flammable. The main gas system feeding the straws is a closed recirculating system. The total gas volume present inside the straws is about $\boldsymbol{39m^3}$. The overall outer envelope of the STT detector is about $\boldsymbol{78m^3}$ and must be sealed from the outside by flushing $\boldsymbol{CO_2}$. One possible issue is related to the leak of $\boldsymbol{CO_2}$ into the near detector hall.

Safety valves must be installed for the STT at the outer edges of the gas seal to prevent the differential pressure between the inside of the STT volume and the outside from exceeding $\boldsymbol{\pm 0.5}$ mbar. More than 3,000 temperature sensors will be distributed in the STT to monitor the temperature of the active detector, as well as that of the front-end electronics and of the cooling circuits. In addition, many parameters of the closed-loop active gas system will be monitored. The gas gain will becontinuously measured by a set of reference straws located outside the STT volume and an automated algorithm will adjust the high voltage on the detector to preserve the stability of the gas gain as the environmental parameters (temperature and/or pressure) change.

4.6 Estimated Cost and Time Scale

The main sub-detector in HiResM$\boldsymbol{\nu}$ is the Straw Tube Tracker, which is also the one in the most advanced design stage. The technology used for this detector is well established and already operational in the ATLAS and COMPASS experiments at CERN. The detailed design of the STT modules foreseen for HiResM$\boldsymbol{\nu}$ is a simple modification of the tracker structure of the constructed wide-aperture magnetic spectrometer in COMPASS. The COMPASS straw tracker uses straws of the same diameter ($\boldsymbol{10mm}$) and has a sensitive area of $\boldsymbol{3.2 \times 2.8\ m^2}$, which is very similar to the one in HiResM$\boldsymbol{\nu}$. In addition, we combine the tracking capability with the particle identication by measuring both drift times and energy loss like in the ATLAS TRT detector. The readout electronic chain and the use of radiators for the Transition Radiation follow closely the ATLAS design. The cost estimate for the STT in HiResM$\boldsymbol{\nu}$ is based upon the actual costs of the ATLAS TRT (straws,

radiators, assembly, readout chain, gas system) and of the COMPASS straw tracker (mechanical frames). Updated quotes from the same vendors who supplied the parts for the ATLAS TRT have been obtained. With the help of the JINR laboratory in Dubna, Russia, which was one of the production centers for both the ATLAS TRT and the COMPASS straw tracker, we prepared a detailed cost estimate including all items needed for the construction of the actual detector. It must be noted that straw modules very similar to the ones foreseen for HiResM$\boldsymbol{\nu}$ have already been built and used in several detectors. Taking advantage of the extensive experience with such detectors, not only we prepared a baseline design for the STT, but we could also reduce the risks on the corresponding cost estimates, as can be seen in Table 2. Overall, the cost of the STT is estimated to be \$12,000,000. including both materials and labor, with an additional 15% contingency (see Table 3).

For the dipole magnet we use the UA1 magnet as reference (also used by NOMAD and T2K ND280) and we scale the corresponding dimensions to the ones of the magnetized volume required by HiResM$\boldsymbol{\nu}$. Our cost estimate is based upon the actual costs of two large aperture dipole magnets built for experiments at CERN: a) the UA1 dipole magnet and b) the more recent LHCb dipole magnet. It is interesting that the costs of these two existing magnets, which are characterized comparable magnetized volumes, are similar, in spite of the different designs and of the fact a long period of time elapsed between them. The designs of both the UA1 and the LHCb dipole magnets are significantly more complex than the one foreseen for HiResM$\boldsymbol{\nu}$, due to special requirements on the shape and field strengths. Another important element to consider is the maximal field $\boldsymbol{B_{\mathbf{max}}}$ achievable, since the cost is roughtly proportional to the value of $\boldsymbol{B_{\mathbf{max}}}$. The nominal field in HiResM$\boldsymbol{\nu}$ will be 0.4 T, but we plan to design the magnet with $\boldsymbol{B_{\mathbf{max}} \sim 0.6}$ T in order to allow some flexibility on the detector parameters. This value is lower than the $\boldsymbol{B_{\mathbf{max}}}$ of both UA1 (0.7 T) and LHCb (1 T) magnets. However, the total magnetized volume is larger in HiResM$\boldsymbol{\nu}$ ($\boldsymbol{4.5 \times 4.5 \times 8\ m^3}$) than in the UA1 magnet ($\boldsymbol{3.5 \times 3.5 \times 7\ m^3}$) by a factor of 1.9. In consideration of the simplified design and of the lower $\boldsymbol{B_{\mathbf{max}}}$, it seems nevertheless safe to evaluate the cost of the HiResM$\boldsymbol{\nu}$ magnet on the basis of the UA1 and LHCb ones. The overall cost is estimated to be \$6,000,000. including material and labor. Since this cost is a top-down estimate from previous experiments without a detailed itemized design, the associated contingency is about 28%, which is larger than the one of the STT.

The design of the electromagnetic calorimeter (ECAL) is still under development since so far we mainly focused on the STT. For the cost estimate we use as a reference the electromagnetic calorimeter built for the T2K ND280 detector, which was mounted inside the UA1 magnet and has a geometry similar to the HiResM$\boldsymbol{\nu}$ one. The T2K calorimeter is a lead-scintillator sampling calorimeter, $\boldsymbol{10X_0}$ thick, which is indeed instrumenting both the sides of the UA1 magnet and the forward region, providing a hermetic coverage of the detector. Due to the higher neutrino energy in LBNE compared to T2K, we would need a deeper ECAL, from $\boldsymbol{10X_0}$ to about $\boldsymbol{18X_0}$, depending upon the longitudinal position inside the magnet. We therefore scale the costs of the T2K design both by the total area we want to instrument and by the increased thickness. It must be noted that the total area covered by the sides is about $\boldsymbol{120m^2}$, while the area of the forward ECAL region is only only $\boldsymbol{16m^2}$. The large ECAL area required to fully instrument the sides of the magnet implies the overall cost of ECAL is dominated by this part. However, the ECAL instrumenting the sides is also more problematic due to the lower average energy of the photons, the presence of material from the STT frames in front of the side ECAL and the higher pile-up rates from events occurring in the return yoke of the magnet. It seems therefore reasonable to stage the contruction of ECAL and/or to partially instrument the sides of the magnet with ECAL. The highest priority should be given to the forward ECAL, followed by the downstream region of the magnet sides. Our

cost estimate assumes to instrument the forward region and the sides for the last downstream $\mathbf{3}\boldsymbol{m}$ with the ECAL of constant thickness of $\mathbf{18}\boldsymbol{X_0}$. The total cost amounts to \$10,800,000. including material and labor. We assign a higher contingency of 43% to the ECAL cost, in consideration of the fact we have only a conseptual design at this stage and we top-down the cost from the T2K design.

For the muon system we have only a conceptual design based upon the NOMAD experience for the moment. The main differences between HiResM$\boldsymbol{\nu}$ and NOMAD are that in HiResM$\boldsymbol{\nu}$ we plan to instrument the sides of the magnet as well in addition to the forward region and that we will use inexpensive RPCs instead of drift chambers. Our rough cost estimate is based upon the cost of the RPCs and the total area instrumented and amounts to \$6,000,000. including material and labor. We assign a large contingency of 45% on this estimate to reflect the preliminary status of the design.

Table 4 summarizes the schedule and the general WBS items for the HiResM$\boldsymbol{\nu}$ detector. The first task is the design and simulation of all sub-detectors which will require approximately 2 years. For the STT this stage has already been started since 01/01/2010, while for the dipole magnet, the ECAL and the muon system it will start next year on 01/01/2011. The detailed engineering including the preparation of the final technical drawings will require one year after the end of the design and simulation and is expected to be completed by 12/31/2012 for the STT and 12/31/2013 for the remaining sub-detectors. The R&D activity will start in parallel with the engineering phase, with the construction and test-beam exposure of prototypes for the STT, the ECAL and the muon system. In the case of the STT we plan to build two different prototypes: a) a half scale prototype of the STT modules to be exposed to test-beams at Fermilab in 2012 and b) a full scale prototypes which should assess the production readiness of the design in 2013. The actual construction of the detector will start on 01/01/2014 with the STT and the dipole magnet and on 01/01/2015 for the ECAL and muon system. The construction phase will last approximately 3 years for the STT, the ECAL and the muon system and 2 years for the magnet. The schedule for the dipole magnet is on a critical path since it must be completed and installed before the installation of the other sub-detectors can take place inside the magnet. The installation of the whole HiResM$\boldsymbol{\nu}$ detector in the near detector hall is expected to be completed by 06/30/2018. Finally, the commissioning will require about 6 months for each sub-detector, so that by 12/31/2018 the HiResM$\boldsymbol{\nu}$ detector will be fully operational and ready to collect data. The construction phase also includes quality tests of the detector modules.

5 R&D Plans

The primary task of HiResMnu is to reduce systematic uncertainties in the neutrino oscillation searches, including those unforeseen by the PMNS mixing matrix, performed by the LBNE at DUSEL. Concurrently, the ND will offer a generational advance in the precision searches and measurements in neutrino physics. To this end, the high resolution tracking capability within a light target, the presence of the magnetic field, and electron-ID are the three crucial ingredients. The optimization of the detector performance and of the sensitivity to oscillations achievable by the LBNE will require detailed simulations. We plan to study the physics potential of HiResMnu by performing a full simulation of the detector response and of the physics processes expected in neutrino interactions. We shall validate our detector simulations against the results of the STT test beam exposure. We will also use the existing neutrino data from the NOMAD experiment to cross-check our results and simulations of neutrino interactions. To establish the HiResM$\boldsymbol{\nu}$ concept

Item	Risks				Weights				Contingency
	Technical	Cost	Schedule	Design	Technical	Cost	Schedule	Design	(%)
Straw Tube Tracker	3	3	2	4	2	1	1	1	15
Dipole Magnet	3	10	4	8	2	1	1	1	28
Electromagnetic Calorimeter	3	10	2	15	2	2	1	1	43
Muon System	4	10	2	15	2	2	1	1	45

Table 2: Summary of risks and corresponding weights to estimate the contingency on the cost of the HiResM$\boldsymbol{\nu}$ detector.

Item	Material (k$)	Labor (k$)	Contingency (k$)	Sum (k$)	Comments
Straw Tube Tracker	10,000	2,000	1,800	13,800	Based upon ATLAS and COMPASS detectors
Dipole Magnet	5,000	1,000	1,680	7,680	Based upon UA1 and LHCb magnets
Electromagnetic Calorimeter	9,000	1,800	4,644	15,444	Based upon T2K electromagnetic calorimeter
Muon System	5,000	1,000	2,700	8,700	
Total	29,000	5,800	10,824	45,624	

Table 3: Summary of the cost estimate for the construction of the HiResM$\boldsymbol{\nu}$ detector.

Item	WBS	Start	Finish	Material (k$)	Labor (k$)	Contingency (k$)	Sum (k$)	Comments
STT	**1.3.4.2.3.1**	**01/01/2010**	**06/30/2018**					
Design and simulation	1.3.4.2.3.1.1	01/01/2010	12/31/2011					
Engineering	1.3.4.2.3.1.2	01/01/2012	12/31/2012					
Prototype 1/2 scale	1.3.4.2.3.1.3	01/01/2011	12/31/2011	204	36	36	276	
Test-beam exposure	1.3.4.2.3.1.4	01/01/2012	12/31/2012					
Prototype full scale	1.3.4.2.3.1.5	01/01/2013	12/31/2013	530	106	95	731	
Production	1.3.4.2.3.1.6	01/01/2014	12/31/2016	10,000	2,000	1,800	13,800	
Installation	1.3.4.2.3.1.7	01/01/2017	12/31/2017					
Commissioning	1.3.4.2.3.1.8	01/01/2018	06/30/2018					
Dipole Magnet	**1.3.4.2.3.2**	**01/01/2011**	**12/31/2016**					
Design and simulation	1.3.4.2.3.2.1	01/01/2011	12/31/2012					
Engineering	1.3.4.2.3.2.2	01/01/2013	12/31/2013					
Production	1.3.4.2.3.2.3	01/01/2014	12/31/2015	4,500	900	1,512	6,912	
Installation	1.3.4.2.3.2.4	01/01/2016	06/31/2016					
Commissioning	1.3.4.2.3.2.5	07/01/2016	12/31/2016					
ECAL	**1.3.4.2.3.3**	**01/01/2011**	**12/31/2018**					
Design and simulation	1.3.4.2.3.3.1	01/01/2011	12/31/2012					
Engineering	1.3.4.2.3.3.2	01/01/2013	12/31/2013					
Prototype	1.3.4.2.3.3.3	01/01/2013	12/31/2013	450	90	230	770	
Test-beam exposure	1.3.4.2.3.3.4	01/01/2014	12/31/2014					
Production	1.3.4.2.3.3.5	01/01/2015	06/30/2017	9,000	1,800	4,644	15,444	
Installation	1.3.4.2.3.3.6	07/01/2017	06/30/2018					
Commissioning	1.3.4.2.3.3.7	07/01/2018	12/31/2018					
Muon System	**1.3.4.2.3.4**	**01/01/2011**	**12/31/2018**					
Design and simulation	1.3.4.2.3.4.1	01/01/2011	12/31/2012					
Engineering	1.3.4.2.3.4.2	01/01/2013	12/31/2013					
Prototype	1.3.4.2.3.4.3	01/01/2013	12/31/2013	350	70	189	609	
Test-beam exposure	1.3.4.2.3.4.4	01/01/2014	12/31/2014					
Production	1.3.4.2.3.4.5	01/01/2015	06/30/2017	5,000	1,000	2,700	8,700	
Installation	1.3.4.2.3.4.6	07/01/2017	06/30/2018					
Commissioning	1.3.4.2.3.4.7	07/01/2018	12/31/2018					

Table 4: Cost and schedule for the construction of the HiResMν detector.

and optimize the detector design, we list tasks in order of priority.

5.1 Simulation Studies

We need a detailed GEANT based simulation of the proposed detector and various options. Professors Mishra, Petti, and Rosenfeld will be the leaders of this project. Collectively they have a long history of participation in of $\boldsymbol{\nu}$-physics projects including CCFR, NOMAD, DONUT, MINOS, and NO$\boldsymbol{\nu}$A. At present commitments to the ongoing MINOS experiment and fabrication of the NO$\boldsymbol{\nu}$A apparatus between them saturate the effort of our post-docs and students.

For the proposed LBNE simulation studies we need at a minimum an additional FTE of post-doctoral effort and one FTE of graduate student effort in 2010. In practice two post-docs will each spend 50% of their time on the LBNE-simulation and the other 50% on the NO$\boldsymbol{\nu}$A and MINOS experiments where the Carolina group is heavily engaged. We anticipate that the student will spend her first year or two on the simulation task and then migrate to a NuMI experiment to complete her thesis. To itemize the support we seek:

- Support for one FTE post-doc and one full-time graduate student.
- Travel support for five physicists to attend LBNE collaboration meetings and to travel to collaborating institutions for a total of twenty trips
- Two computing nodes and associated disk storage for these simulations. We will augment our computing with the existing facilities at Carolina.

Thus far, we have used a parametrized fast simulation. Fortunately, the NOMAD data serve as a very important calibration for the calculation. These data will continue an an important guide in the simulation studies.

5.2 STT Prototype

Having optimized the detector parameters and established consensus in the LBNE collaboration, we plan to build a prototype straw tube tracker (STT) module. We envision to undertake this task in the second or third year of this proposal. As described in Section 2, the STT technology is well established and demonstrated to be reliable in the ATLAS and COMPASS experiments at CERN. Therefore, the STT prototype is intended to test and optimize the actual module design and the readout chain foreseen for HiResM$\boldsymbol{\nu}$, and to measure the corresponding performance in terms of tracking capability and particle identification. We plan to expose the STT prototype to test beams at Fermilab or CERN, and to test different options for the readout electronics and the module mechanics. The prototype will have an active area of $\mathbf{1.8}\boldsymbol{m} \times \mathbf{1.8}\boldsymbol{m}$, but other than the overall dimensions it shall follow the exact same design of the HiResM$\boldsymbol{\nu}$ modules. We plan to build three STT modules, each of them composed by a double layer of straws, a radiator and the electronic readout. This will provide a total of six space points per module to reconstruct track parameters.

The STT prototype will be assembled at the University of South Carolina and will then be sent to Fermilab for the test beam exposures. The JINR laboratory in Dubna, Russia will provide technical support during the construction of the STT prototype. The project can thus take advantage of the large experience the JINR laboratory has accumulated as one of the main production centers for the ATLAS TRT detector and for the COMPASS straw tube tracker. We plan to produce three STT double layers in the period between CD-1 and CD-2 (starting FY11). The estimated cost for the construction of the STT prototype is summarized in Table 5. The budget request for the

STT fabrication is based upon the actual costs of similar straw detectors built for the ATLAS and COMPASS experiments at CERN. The cost includes variations on the STT design aimed to teach us both the test-beam response and the optimization of the sub-detector to save us cost during mass production. Overall, the total cost to construct the STT prototype amounts to $484,000. + $73,000 (15%) contingency during the R&D measurements. Although on the equipment purchase above $5000 there will be no indirect cost, the personnel involved in the construction will incur an indirect of 26%; this cost has not been included in the budget. (We deem it to be small.) We envision that the R&D effort will take three years from the start date.

Item	Cost ($)
Mechanics	144,000
Carbon bars	50,000
Straws	35,000
End-plug with contact elements	6,000
Spacers	8,000
Crimping pins	8,000
Motherboards	10,000
Consummable material	15,000
Mounting tooling and equipment	35,000
Gas system	25,000
Front end electronics + ATLAS ASIC	25,000
Back end electronics	13,000
HV power supply	12,000
LV power supply	10,00
Cabling	7,000
Patch panels	1,000
Labor	80,000
Total	484,000
Contingency 15%	73,000

Table 5: Summary of the STT R&D budget request in preparation for CD-2.

5.2.1 A Full Scale STT-Module Construction

We plan to build one full scale STT module during the R&D work. We do not anticipate to expose the full scale module to the test beam. However, it is important to establish the detailed modus operandi for the mass production of the STT. Our estimate to fabricate one full scale STT is about $450,000.

5.3 ECAL Prototype

Our default ECAL design is based upon the lead-scintillator calorimeter used in the T2K-ND280 detector. For ECAL, the most important region is the downstream end of the detector — we propose to build this in the first stage. The ECAL will have transverse and longitudinal segmentation. We propose to build a 10 X0 deep calorimeter with lead (1.75mm) and scintillator (4cm x 1cm) sampling in the downstream region. The estimated cost of the downstream ECAL will be about

$3M. In the second stage, we plan to instrument the sides, 5 X0 deep with coarser granularity which will make the detector hermetic. The cost of partially instrumenting the sides is about $3M.

The ECAL R&D effort will be begin a year after STT, and two years after simulation studies, and will last about two to three yeras. The ECAL task will be lead by a group(s) other than Carolina. We anticipate that the ECAL R&D cost will be about $500,000.

5.4 Dipole Magnet

The proposed dipole magnet a larger version than the UA1 dipole magnet which was used by NOMAD. Figure 27 shows the magnet yoke assembly, Figure 28 shows the yoke & coils, Figure 29 shows the coil assembly, and Figure 30 shows the specifications of the UA1 magnet. Table 6 summarizes the salient parameters of this magnet at maximum operating B-field of 0.7 T. The HiResMnu magnet will operate at 0.4T.

Item	Cost ($)
Dimension	3.5 x 3.5 x 7 m^3
Maximum B-Field	0.7 T
Maximum Current	10,000 A
Resistance (40C)	0.0576
Voltage	576 V
Mass	900 T
Cooling water flow	50 liters/sec
Pressure gredient	15 atm (in .vs. out)
Temperature Diff	30 C

Table 6: Parameters of the UA1 Dipole magnet. The quoted numbers are for Al-coil and the maximum B-field (0.7 T). The nominal B-field for HiResMnu is 0.4 T.

The main differences between the UA1 and the HiResMnu magnet are: **(a):** Size; **(b):** Coil — UA1 used Al-coil (to minimize the degradation of the energy resolution of the outgoing jets) whose resistivity $\rho_{Al} = 2.8 \times 10^{-8} \Omega m$ whereas the HiResMnu will use Cu-coil whose conductivity is $\rho_{Al} = 1.7 \times 10^{-8} \Omega m$; and **(c):** HiResMnu magnet does not need a hole in the coil as was the case with the UA1 magnet.

We estimate the cost of the HiResMnu magnet to be $5M with an additional $1.25M (25%) as labour. We do not think that much R&D is needed to fabricate the new magnet.

5.5 Muon Detector

In the HiResMnu design, the muon-detectors will identify muon-tracks which will then be matched with the STT tracks with measured momenta and charges. The muon detectors thus are not required to furnish muon momentum, only the μID. However, given the large rate of muons in the ND location, we do need μ-detectors with good spatial ($\approx 200\mu$) and time ($\approx$ a few ns) resolution to effect a good match with the STT tracks.

Two types of muon detectors will be employed in the proposed detectors. First, we plan to instrument the magnet yoke with the muon-range detectors (MRD) which will offer μID at low momentum, down to 200 MeV. Second, there will be large muon detectors outside the magnet at 5λ and 8λ respectively to identify the high energy muons. (NOMAD only used the large muon detectors outside the magnet).

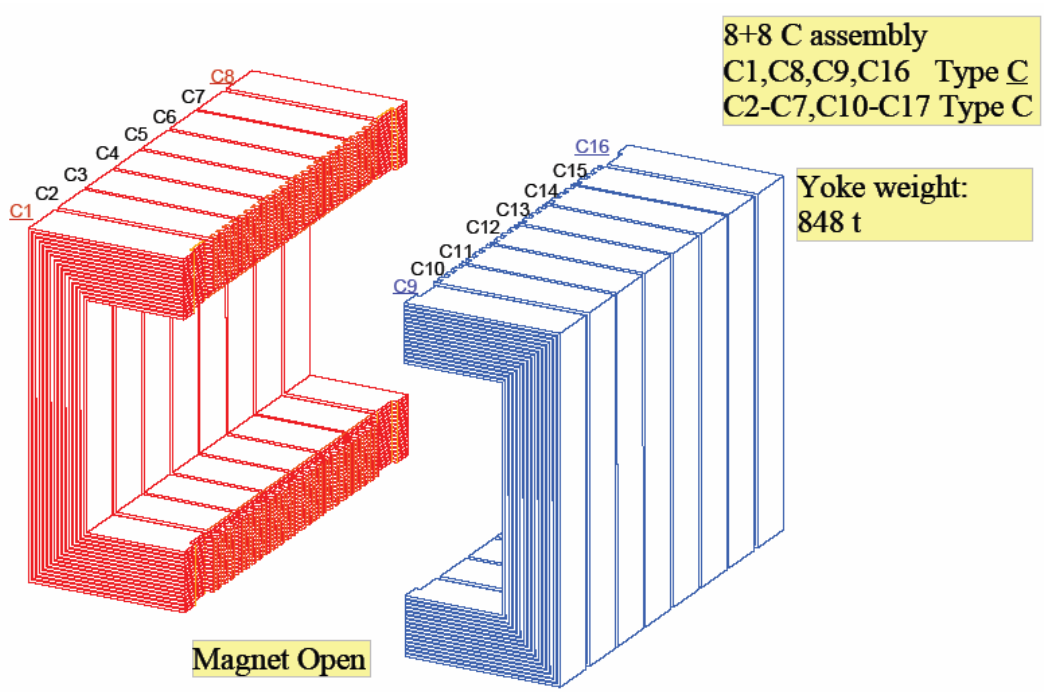

Figure 27: Magnet yoke assembly of the UA1 dipole magnet.

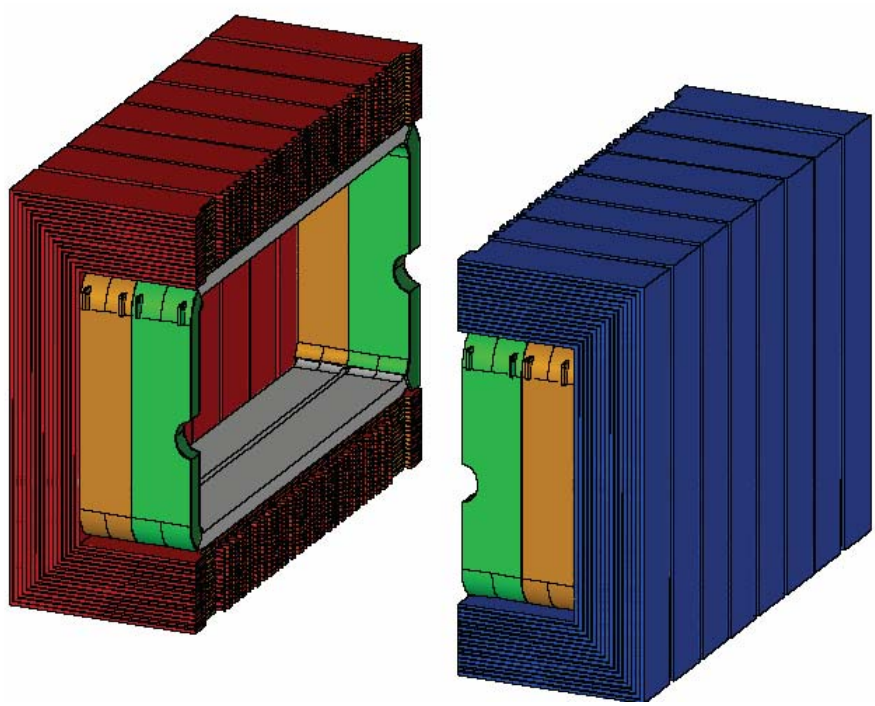

Figure 28: Yoke and coil of the UA1 dipole magnet.

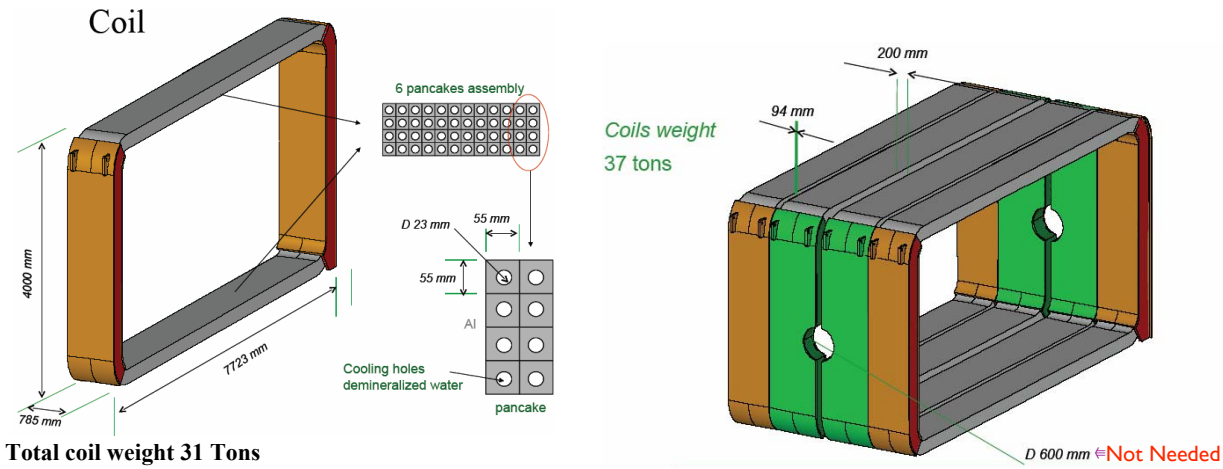

Figure 29: Coil and coil-assembly of the UA1 dipole magnet.

Figure 30: Specs of the UA1 dipole magnet.

Inexpensive RPC's are the choice of the muon-detectors. Our calculations show that they will survive the rate and provide the $\boldsymbol{\mu}$ID with adequate precision. The cost of muon detector is estimated at $5M with labor. The R&D cost of the muon detector is estimated at $500k. We anticipate that the muon detector effort will be lead by institutions other than Carolina. The R&D effort will begin concurrently with the ECAL work, about two years after the simulation studies.

References

[1] S. Mishra, R. Petti and C. Rosenfeld, Letter of Intent submitted to Fermilab, February 2008, `http://www.fnal.gov/directorate/Longrange/Steering_Public/community_letters.html`;

S. Mishra, R. Petti and C. Rosenfeld, Proceedings of the Nufact08 conference - Valencia Spain, June 30 - July 5 2008, PoS SISSA 069 (2008), arXiv:0812.4527 [hep-ex]; to be submitted to NIM.

[2] J. Altegoer et al. [NOMAD collaboration], Nuclear Instruments and Methods A 404 (1998) 96-128.

[3] P. Astier et al. [NOMAD collaboration], Nucl. Phys. B611 (2001) 3-39, hep-ex/0106102

[4] P. Astier et al. [NOMAD collaboration], Phys. Lett. B 570 (2003) 19-31, hep-ex/0306037

[5] C.T. Kullenberg et al. [NOMAD collaboration], submitted to Phys. Lett.B; arXiV: 0910.0062v1 [hep-ex]

[6] T. Akesson et al., Nucl.Instrum.Meth. A522 (2004) 131-145

[7] T. Akesson et al., Nucl.Instrum.Meth. A522 (2004) 50-55

[8] T. Akesson et al., IEEE Nucl.Sci.Symp.Conf.Rec.2 (2005) 1185-1190

[9] V.N. Bychkov et al., Particles and Nuclei Letters, 2 (111) June 2002

[10] K. Platzer et al., IEEE Transactions on Nuclear Science, vol. 52, No. 3, June 2005

[11] S.R.Mishra, Review talk presented at *Workshop on Hadron Structure Functions and Parton Distributions*, Fermilab, Apr.1990; World Scientific, 84-123(1990), Ed. D.Geesaman ***et al.***; Nevis Preprint # 1426, Jun(1990);

[12] P. Astier et al. [NOMAD collaboration], Nucl. Phys. B621/1-2 (2001) 3-34, hep-ex/0111057

[13] D. Naumov et al. [NOMAD collaboration], Nucl.Phys.B 700 (2004) 51-68, hep-ex/0409037

[14] Q. Wu et al. [NOMAD collaboration], Phys. Lett. B 660 (2008) 19-25; arXiv:0711.1183 [hep-ex]

[15] Particle Data Group, W.-M. Yao et al., Journal of Physics, G 33 (2006) 1

[16] G. P. Zeller et al. [NuTeV collaboration], Phys. Rev. Lett. **88**, 091802 (2002), arXiv:hep-ex/0110059.

[17] E. A. Paschos and L. Wolfenstein, Phys. Rev. D **7**, 91 (1973).

[18] A. Czarnecki and W.J. Marciano, Int. J. Mod. Phy. A15 (2000) 2365

[19] S.C. Bennet and C.E. Wieman, Phys. Rev. Lett. 82 (1999) 2484

[20] P.L. Anthony et al [E158 collaboration], Phys.Rev.Lett. 95 (2005) 081601, hep-ex/0504049

[21] T. Adams et al. [NuTeV collaboration], Phys.Rev.Lett. 87 (2001) 041801, hep-ex/0104037

[22] A.A. Aguilar-Arevalo et al. [MiniBOONE collaboration], Phys. Rev. Lett. 98 (2007) 231801, arXiv:0704.1500 [hep-ex]

[23] S. Gninenko, arXiv:0902.3802 [hep-ph]

[24] S. Alekhin, S. Kulagin and R. Petti, arXiv:0812.4448 [hep-ph], Physics Letters B 675 (2009) 433-440.

[25] S. Alekhin, S.A. Kulagin and R. Petti, AIP Conf.Proc. 967 (2007) 215-224, arXiv:0710.0124 [hep-ph]

[26] S. Alekhin, S.A. Kulagin and R. Petti, Nuint 07, Fermilab, Batavia, May 30 - June 3 2007, talks in http://conferences.fnal.gov/nuint07/

[27] S. Alekhin, S.A. Kulagin and R. Petti, Proceedings of DIS08 - University College London, April 7-11 2008; arXiv:0810.4893 [hep-ph].

[28] A. B. Arbuzov, D. Y. Bardin and L. V. Kalinovskaya, JHEP **78**, 506 (2005); arXiv:hep-ph/0407203.

[29] K. P. Diener, S. Dittmaier and W. Hollik, Phys. Rev. D **69**, 073005 (2004).

[30] S.A. Kulagin and R. Petti, Nucl. Phys. A 765 (2006) 126-187, hep-ph/0412425

[31] S.A. Kulagin and R. Petti, Phys.Rev. D 76 (2007) 094023, hep-ph/0703033